

Brassinosteroid gene regulatory networks at cellular resolution

Trevor M Nolan^{*1}, Nemanja Vukašinović^{*2,3}, Che-Wei Hsu^{*4,5}, Jingyuan Zhang¹, Isabelle Vanhoutte^{2,3}, Rachel Shahan^{1,9}, Isaiah W Taylor¹, Laura Greenstreet⁶, Matthieu Heitz⁶, Ping Wang⁷, Pablo Szekely^{1,9}, Aiden Brosnan¹, Yanhai Yin⁷, Geoffrey Schiebinger⁶, Uwe Ohler^{4,7,8}, Eugenia Russinova^{2,3,✉}, and Philip N Benfey^{1,9,✉}

^{*}These authors contributed equally

¹Department of Biology, Duke University, Durham, NC 27708, USA

²Department of Plant Biotechnology and Bioinformatics, Ghent University, Ghent, Belgium

³Center for Plant Systems Biology, VIB, Ghent, Belgium

⁴Department of Biology, Humboldt Universität zu Berlin, 10117 Berlin, Germany

⁵The Berlin Institute for Medical Systems Biology, Max Delbrück Center for Molecular Medicine, 10115 Berlin, Germany

⁶University of British Columbia, Department of Mathematics, Vancouver, Canada

⁷Department of Genetics, Development and Cell Biology, Iowa State University, Ames, IA 50011, USA

⁸Department of Computer Science, Humboldt Universität zu Berlin, 10117 Berlin, Germany

⁹Howard Hughes Medical Institute, Duke University, Durham, NC 27708, USA

Brassinosteroids (BRs) are plant steroid hormones that regulate diverse processes such as cell division and cell elongation. BRs control thousands of genes through gene regulatory networks (GRNs) that vary in space and time. We used time series single-cell RNA-sequencing to identify BR-responsive gene expression specific to different cell types and developmental stages of the *Arabidopsis* root, uncovering the elongating cortex as a site where BRs trigger a shift from proliferation to elongation associated with increased expression of cell wall-related genes. Our analysis revealed HAT7 and GTL1 as BR-responsive transcription factors that regulate cell elongation in the cortex. These results establish the cortex as an important site for BR-mediated gene expression and unveil a BR signaling network regulating the transition from proliferation to elongation, illuminating new aspects of spatiotemporal hormone response.

Single-cell RNA-sequencing | time course | gene regulatory networks | brassinosteroid | *Arabidopsis* | root cell elongation | tissue-specific CRISPR

Correspondence: Eugenia.Russinova@psb.vib-ugent.be
Philip.Benfey@duke.edu

Introduction

During development, cells pass through different states as they acquire identities and progress towards end-stage differentiation (Pierre-Jerome et al., 2018). Gene regulatory networks (GRNs) control this progression and must be tuned according to developmental stage, cell identity, and environmental conditions (Levine and Davidson, 2005; Moreno-Risueno et al., 2010; Shahan et al., 2021). Signaling molecules such as hormones are central players in coordinating these networks, but it has been challenging to disentangle how cell identities, developmental states, and hormone responses influence one another. Recent technological advances in single-cell RNA-sequencing (scRNA-seq) (Seyferth et al., 2021; Shahan et al., 2021) and tissue-specific gene manipulations (Decaestecker et al., 2019; Wang et al., 2020) make it possible to address this challenge.

Brassinosteroids (BRs) are a group of plant steroid hormones that affect several aspects of development including cell division, cell elongation and differentiation (Clouse et al., 1996; Li et al., 1996; Szekeres et al., 1996). BRs are

sensed at the plasma membrane by BRI1 family receptors and BAK1/SERK co-receptors (Caño-Delgado et al., 2004; Kinoshita et al., 2005; Li and Chory, 1997; Li et al., 2002), initiating a series of signal transduction events that activate BES1 and BZR1 family transcription factors in the nucleus (Wang et al., 2002; Yin et al., 2002, 2005). BES1 and BZR1 direct BR-responsive GRNs by interacting with other transcription factors to control thousands of genes (Clark et al., 2021; Nolan et al., 2017, 2020; Sun et al., 2010; Yu et al., 2011). This downstream GRN is typically represented singularly without consideration of cell specificity (Clark et al., 2021; Guo et al., 2013; Seyed Rahmani et al., 2021; Yu et al., 2011), but BRs lead to different responses depending on cell type and developmental stage, suggesting that multiple BR GRN configurations exist (Ackerman-Lavert et al., 2021; Fridman et al., 2014; Vilarrasa-Blasi et al., 2014).

The *Arabidopsis* root is well suited to investigate spatiotemporal BR responses (Jaillais and Vert, 2016). Cell types are found on the radial axis of the root and each cell file forms a developmental timeline, with stem cells in the meristem at the tip of the root and more mature cells towards the shoot in the elongation and maturation zones (Dolan et al., 1993). Loss-of-function mutants in the BR pathway have short roots due to impaired cell division and reduced cell elongation (González-García et al., 2011; Kang et al., 2017; Vukašinović et al., 2021), suggesting that BRs play crucial roles in both the meristem and elongation zone. The optimal concentration of BRs varies between these developmental zones (Vukašinović et al., 2021). Relatively low levels of BRs in the meristem are required for cell cycle progression and orientation of cell division planes, but balanced signaling is important as excess BRs result in exit from the cell cycle, premature elongation, differentiation, and exhaustion of the meristem (González-García et al., 2011; Graeff et al., 2021; Li et al., 2021). BR biosynthesis increases along the longitudinal axis of the root, peaking in the elongation zone, where BRs promote cell elongation (Chaiwanon and Wang, 2015; Vukašinović et al., 2021).

BR signaling also varies among cell types. The epidermis is a major site for BR-induced gene expression that controls

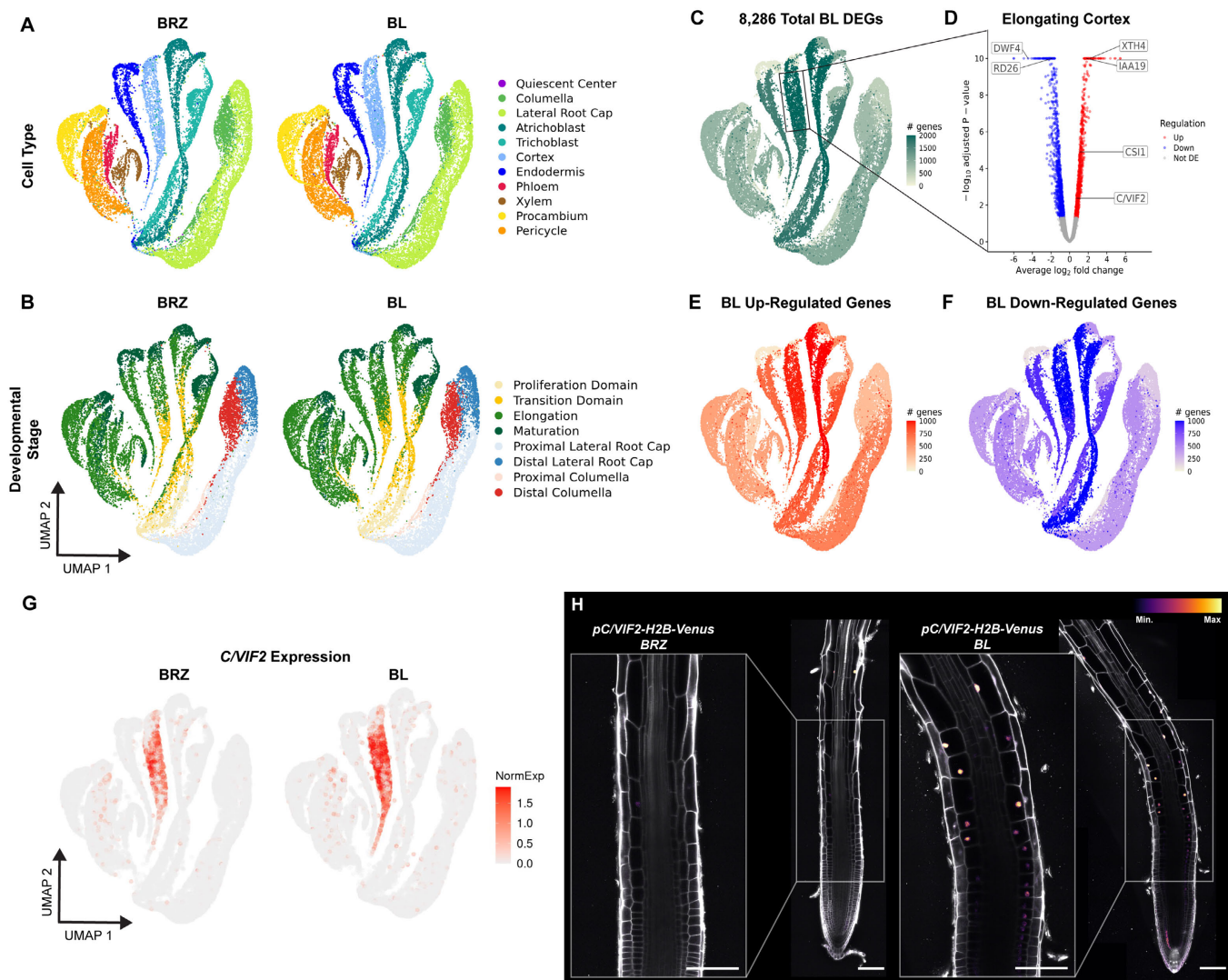


Fig. 1. scRNA-seq identifies the elongating cortex as a site of BR-response.

(A,B) Two-dimensional uniform manifold approximation and projection (UMAP) embedding of 21,473 BRZ and 22,275 two-hour BL treated cells across 3 biological replicates of scRNA-seq. Colors indicate (A) cell type or (B) developmental stage annotation.

(C) Spatiotemporal response to 2 hour BL treatment among each combination of cell type and developmental stage of the root. Color on the UMAP projection indicates the number of differentially expressed genes (DEGs).

(D) Volcano plot of DEGs in the elongating cortex. Color indicates the direction of regulation. Known markers of BR response including *DWF4*, *RD26*, *XTH4* and *IAA19* are indicated. *C/VIF2* and *CS11* (described in this study) are also indicated.

(E, F) UMAP projection colored by BL upregulated DEGs (E) or BL down-regulated DEGs (F).

(G) Expression of *C/VIF2* in BRZ and BL scRNA-seq. The color scale represents log normalized, corrected UMI counts.

(H) *pC/VIF2-H2B-Venus* reporter grown on 1 μ M BRZ for 7 days and transferred to 1 μ M BRZ or 100 nM BL for 4 hours. Inset shows *C/VIF2* signals in the elongating cortex that increase with BL treatment. Propidium iodide-staining is shown in grey, with the color gradient indicating relative *C/VIF2-H2B-Venus* levels. Scale bars, 100 μ m.

BL, brassinolide; BRZ, brassinazole.

meristem size (Ackerman-Lavert et al., 2021; Belkhadir and Jaillais, 2015; Chaiwanon and Wang, 2015; Fridman et al., 2014, 2021; González-García et al., 2011; Hacham et al., 2011; Jaillais and Vert, 2016; Nolan et al., 2020; Planas-Riverola et al., 2019). On the other hand, BR-regulated genes in the stele tend to be repressed and are implicated in differentiation and radial expansion (Fridman et al., 2021; Kang et al., 2017; Vragović et al., 2015). Additionally, BRs promote divisions of quiescent center cells via interactions of BES1 with BRAVO, a quiescent center-enriched transcription factor (Betegón-Putze et al., 2021; Lozano-Elena et al., 2018; Vilarrasa-Blasi et al., 2014). This suggests that BR GRNs involve context-specific transcription factors, but BR responses

have so far been characterized in only a handful of cell types. Since BR responses vary according to both cell type and developmental stage, increased resolution is needed to understand how spatiotemporal BR GRNs are wired.

scRNA-seq can provide such resolution and is a powerful approach to investigate cell- and developmental-stage-specific responses (Seyfferth et al., 2021; Shahan et al., 2021). Droplet-based scRNA-seq enables profiling thousands of Arabidopsis root cells (Denyer et al., 2019; Jean-Baptiste et al., 2019; Ryu et al., 2019; Shulze et al., 2019; Wendrich et al., 2020; Zhang et al., 2019). Using this technology, we constructed a single-cell reference atlas that captures the major cell types and developmental stages of the

Arabidopsis root (Shahan et al., 2022). This atlas allows the investigation of fine-scale transitions at a resolution beyond the morphologically defined meristem, elongation, and maturation zones and facilitates the analysis of additional single-cell experiments through annotation label transfer (Shahan et al., 2022; Stuart et al., 2019). Although scRNA-seq has been used to profile mutants (Denyer et al., 2019; Ryu et al., 2019; Shahan et al., 2022) and investigate plant responses to the environment (Jean-Baptiste et al., 2019; Shulze et al., 2019), previous studies have profiled a single time point and have not explored the GRNs that mediate stimuli-specific responses.

In this study, we used scRNA-seq to profile BR responses across the majority of cell types and developmental stages of the root. We discovered that BRs strongly affect gene expression in the elongating cortex. A BR scRNA-seq time course and reconstruction of cortex trajectories showed that BRs trigger a shift from proliferation to elongation, which is associated with up-regulation of cell wall-related genes. Accordingly, loss of BR signaling in the cortex had little effect on meristem cell length but reduced cell expansion in the elongation zone. Our time-course data allowed us to infer BR-responsive GRNs across cell types, developmental stages, and time points, which led to the identification of HAT7 and GTL1 as validated regulators of BR response in the elongating cortex. These datasets represent more than 180,000 single-cell transcriptomes, providing a view of BR-mediated GRNs at unprecedented resolution.

Results

Reference-guided scRNA-seq reveals differential brassinosteroid response in the Arabidopsis root

To investigate spatiotemporal BR responses in the root, we used a sensitized system. We first inhibited endogenous BR biosynthesis using Brassinazole (BRZ) (Asami et al., 2000) and then reactivated signaling by treating with Brassinolide (BL), the most active BR (Clark et al., 2021; Grove et al., 1979; Nolan et al., 2020). We treated 7-day-old primary roots for 2 hours with BL or a corresponding mock BRZ control and performed scRNA-seq on protoplasts isolated from 0.5cm root tips (containing meristem, elongation and early differentiation zones) using the 10X Genomics Chromium system (Methods). Employing Cell preproCessing Pipeline kaLlistO busTools (COPILOT) (Bray et al., 2016; Melsted et al., 2019; Shahan et al., 2022), which streamlines scRNA-seq data processing and quality control, we identified over 43,000 high-quality cells with approximately equal numbers for each treatment (Figures 1A-B and Data S1).

To annotate the cell types and developmental stages, we performed label transfer implemented in Seurat (Stuart et al., 2019) based on our single-cell expression atlas of the Arabidopsis root (Shahan et al., 2022). To follow the developmental progression from the meristem to the elongation zone more closely, we distinguished between two domains of the meristem: the proliferation domain, where cells have a high probability to divide, and the transition domain, where cells divide less frequently but have not yet begun rapid cell expansion

(Figures S1A-D and Data S2) (Ivanov and Dubrovsky, 2013; Salvi et al., 2020).

After data integration, the 11 major cell types and eight developmental stages identified were logically arranged in 2D uniform manifold approximation and projection (UMAP) space as we and others have previously described for root datasets (Figures 1A and 1B; (Denyer et al., 2019; Shahan et al., 2022). More specifically, young cells in the proliferation domain group together, indicating their transcriptional similarity. As cells develop, they become transcriptionally distinct and separate in UMAP space, forming four major branches corresponding to the stele, the ground tissue which includes cortex and endodermis, the epidermis and root cap (Dolan et al., 1993; Shahan et al., 2022). Marker genes characteristic of cell types and developmental stages remained enriched as expected, suggesting that although BRs alter the expression of thousands of genes, cell identities can be successfully aligned through integration (Figure S2A and S2B).

scRNA-seq captures spatiotemporal patterns of BR-responsive gene expression

Previous studies have profiled BR-responsive gene expression in bulk tissue or in a handful of cell types, conflating cell type and developmental stage (Chaiwanon and Wang, 2015; Guo et al., 2013; Vragović et al., 2015). To obtain better spatiotemporal resolution of the BR response, we performed differential expression analysis for each combination of cell type and developmental stage using pseudobulk expression profiles (Crowell et al., 2020); see methods). We identified over 8,000 differentially expressed genes (DEGs; Fold-change >1.5, False discovery rate <0.05; Figures 1C-F), which were enriched in BES1 and BZR1 targets and had significant overlap with previously identified BR-regulated genes (Figures S2C, S2D and Data S3).

Strikingly, we found that 37% of DEGs were significantly altered in a single cell type/developmental stage and more than 82% were differentially expressed in 5 or fewer cell type/developmental stage combinations (Figure S2E). This indicates that although BRs broadly influence gene expression, they modulate distinct sets of genes in different spatiotemporal contexts.

Among the tissues with many DEGs was the epidermis, as previously described (Chaiwanon and Wang, 2015; Fridman et al., 2014; González-García et al., 2011; Hacham et al., 2011). Trichoblasts, or non-hair cells in the epidermis were particularly affected, showing marked changes across both the meristem and elongation zone. Unexpectedly, our data also indicated that BRs strongly influence gene expression in the cortex, especially in the elongation zone (Figures 1C and S2D). The cortex has been linked to plant environmental interactions, including response to water limitation (Longkumer et al., 2021; Verslues and Longkumer, 2022) and hydrotropism (Dietrich et al., 2017; Miao et al., 2021; Takahashi et al., 2002), but how BRs modulate gene expression in the cortex and what processes are affected have not been described. To address these questions, we focused

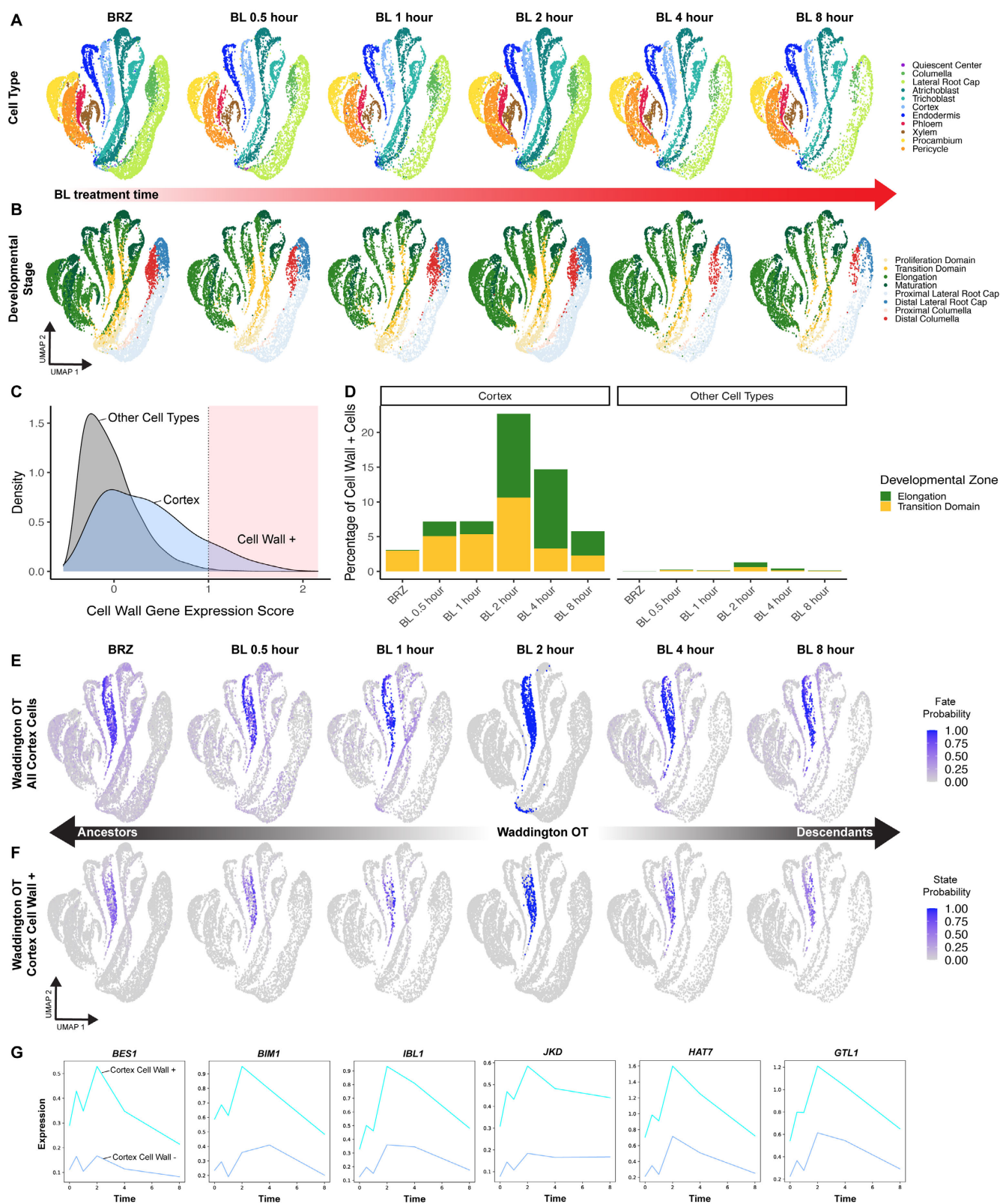


Fig. 2. Waddington optimal transport traces cortex trajectories along a BR scRNA-seq time series.

(A) UMAP of 52,921 cells across 6 time points of a scRNA-seq BL treatment time course. Mock BRZ control represents time 0. Colors indicate cell type annotation.

(B) UMAP projection colored by developmental stage annotation.

(C) Density plot showing cell wall gene expression score. The shaded region with cell wall expression scores >1 indicates "Cell Wall+" cells.

(D) Bar plot showing the percentage of Cell Wall+ cells in the cortex versus other cell types over the time course. Color indicates developmental stage annotation. Only transition and elongation zones are shown as other zones represent less than 2% of cell wall + cells.

(E) WaddingtonOT (WOT) fate probabilities for all cortex cells along the BL time course. The BL 2 hour time point was used as a reference, therefore all cells have a probability of either 1 or 0 at this time point.

(F) Probabilities for cortex cell wall+ state from WOT trajectories.

(G) Expression trends for select transcription factors differentially expressed along WOT cortex cell wall+ trajectories.

on BR-mediated gene expression in the elongating cortex.

Cell wall-related genes are up-regulated by BRs in the elongating cortex

We found that BR treatment led to approximately 1,000 up-regulated genes and about the same number of down-regulated genes in the elongating cortex (Figures 1D and S2D). Gene ontology (GO) analysis indicated the BR up-regulated genes were strongly enriched for genes related to “cell wall organization or biogenesis”, which is intriguing given the role of BRs in promoting cell elongation (Figure S2F). The cell wall-related DEGs included *CELLULOSE SYNTHASES* (*CESAs*), *CELLULOSE SYNTHASE INTERACTIVE1* (*CSII*), which is required for efficient cellulose synthesis and alignment of cellulose synthase complexes with cortical microtubules (Bringmann et al., 2012; Gu et al., 2010; Li et al., 2012) and cell-wall loosening enzymes such as *EXPANSINS* and *XYLOGLUCAN ENDOTRANSGLUCOSYLASES*. Cell-wall-related genes such as *CESAs* have been demonstrated to be direct targets of BES1 and BZR1 (Sun et al., 2010; Xie et al., 2011; Yu et al., 2011), but their spatiotemporal regulation, especially in the cortex, has not been reported.

To monitor their responsiveness to BRs, we generated transcriptional reporters for three of the DEGs: *C/NIF2*, *CSII* and *XTH16*. *CELL WALL / VACUOLAR INHIBITOR OF FRUCTOSIDASE 2* (*C/NIF2*) was enriched in the transition domain and elongation zone of the cortex and induced by BL (Figures 1G-H). *CSII* was broadly induced by BL, especially in the epidermis and cortex (Figures S2G and S2H). *XYLOGLUCAN ENDOTRANSGLUCOSYLASE/HYDROLASE 16* (*XTH16*) was enriched in the endodermis and induced by BL (Figures S2I and S2J). These results confirm that our differential expression analysis captures spatiotemporal BR responses and raises the possibility that BR induction of cell-wall-related genes is associated with cortex cell elongation.

Waddington optimal transport identifies exceptionally responsive cells in a BR scRNA-seq time course

Analyzing expression trends over a time course can reveal regulators and downstream targets associated with gene expression programs (Schiebinger, 2021; Swift et al., 2021). A recently developed analytical approach for scRNA-seq is Waddington-OT (WOT), which connects snapshots of gene expression along a time course to facilitate trajectory reconstruction (Schiebinger et al., 2019). WOT identifies putative ancestors for a given set of cells at earlier time points and descendants at later time points (Schiebinger et al., 2019; Shahan et al., 2022; Zhang et al., 2021).

To better understand how BRs influence cell wall-related gene expression we performed scRNA-seq at six time points beginning with BRZ treatment (time 0) and subsequent BL treatments for 30 minutes, 1 hour, 2 hours, 4 hours or 8 hours (Figures 2A and 2B). These time points capture the rapid root elongation triggered by re-addition of BRs (Chaiwanon and Wang, 2015).

To examine the trajectories leading to activation of cell wall-related genes in the elongating cortex, we applied WOT (Schiebinger et al., 2019) and created a cell wall gene signature using 107 cell wall-related genes that were induced by BL in the elongating cortex (Data S4). We monitored the relative expression of this set of genes, resulting in a “cell wall score” for each cell in the time course (see methods). Cortex cells had a higher cell wall score compared to other cell types, which increased with BL treatment (Figures 2C-D and S3A-B), confirming that the cell wall score represents a BR-responsive module in the cortex. At the 2 hour BL time point, more than 20% of cortex cells had a cell wall score greater than 1, whereas only 5% or fewer cells in other cell types exhibited scores this high (Figure 2C). We therefore designated cells with a cell wall score of at least 1 as “Cell wall+” to indicate their exceptional BR response (Figures 2C-D).

BR induction of cell wall genes in the cortex is associated with the switch to elongation

An advantage of WOT analysis is that it does not rely on pre-specified boundaries between developmental zones. We used this property to examine the relationship between developmental stage annotation and cell wall score. Under BRZ treatment, cortex cell wall+ cells were sparse and predominantly annotated as transition domain. Upon BL treatment, the annotation of cortex cell wall+ cells shifted to the elongation zone (Figure 2D), suggesting that BR induction of cell wall-related genes is related to the onset of cell elongation.

Using the cells at the 2 hour time point as a reference, we looked at the probability of cells being ancestors or descendants of cortex cell wall+ cells. We also constructed a similar trajectory for the remaining cortex cells, which were designated “cortex cell wall-”. These trajectories illustrated a shift towards the cortex cell wall+ state upon BL treatment that coincided with a change from transition domain to elongation zone annotation (Figures 2D-F). These results provide support for the hypothesis that BRs are involved in initiating elongation of cortex cells via activation of cell wall genes.

Differential expression along WOT trajectories identifies BR-responsive transcription factors

To reveal potential regulators of cell wall-related genes in the cortex, we performed probabilistic differential expression analysis along WOT trajectories, contrasting cells assigned to cortex cell wall+ versus cortex cell wall- states at each time point (see methods). Among the DEGs identified were known transcription factors in the BR pathway including *BES1* (Yin et al., 2002), *BIMI* (Yin et al., 2005), and *IBL1* (Zhiponova et al., 2014); Figure 2G and Data S4). We also identified additional transcription factors whose role in the BR pathway has not been examined in detail (Figure 2G). These include *JACKDAW* (*JKD*), which is involved in ground tissue specification (Moreno-Risueno et al., 2015), *HAT7/HB-3*, an uncharacterized class I HD-ZIP TF (Ariel et al., 2007; Henriksson et al., 2005; Mattsson et al., 1992) and *GTL1*, which negatively regulates growth in trichomes

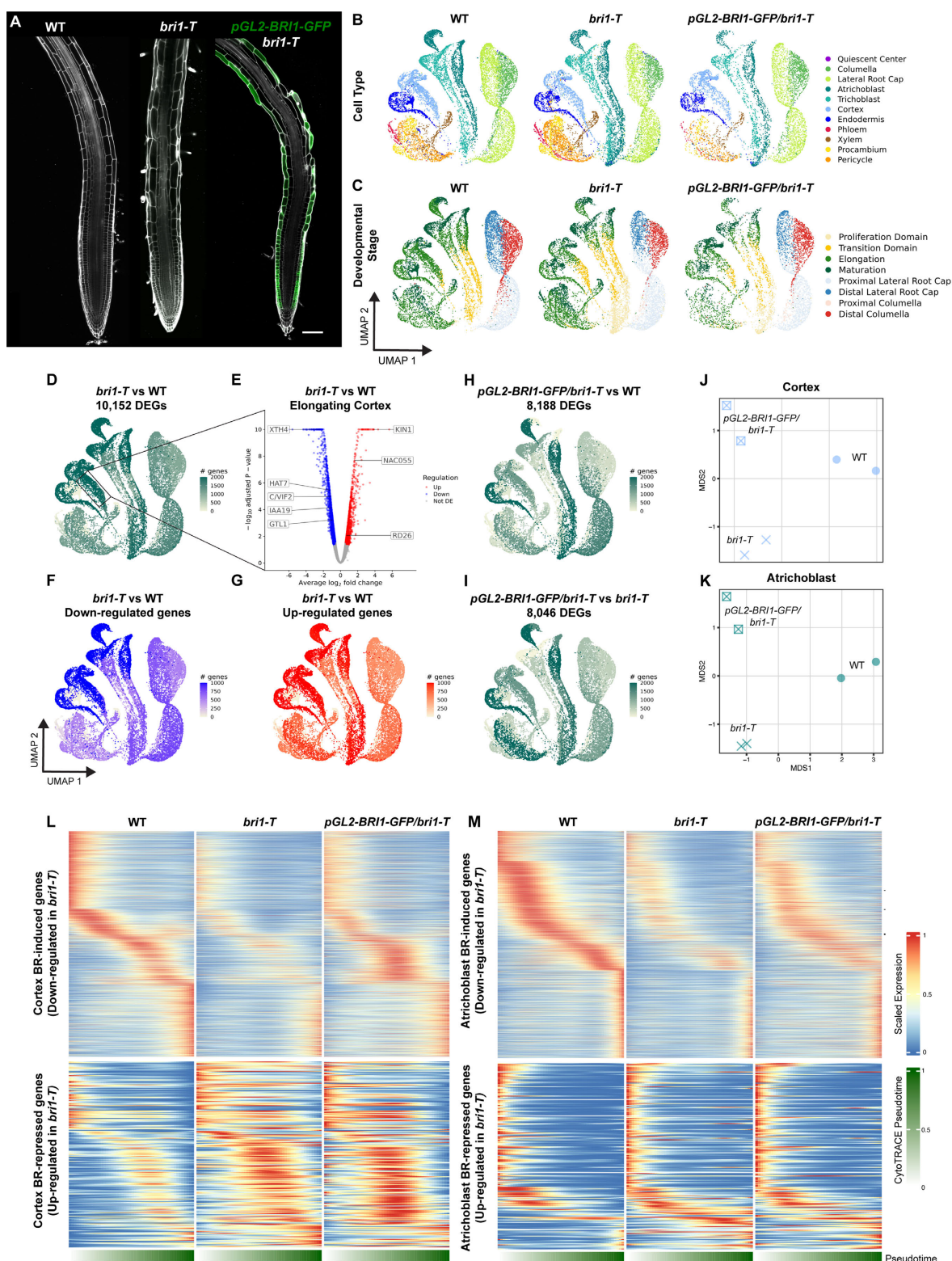


Fig. 3. Triple receptor mutant *bri1-T* gene expression changes in cortex and distinct patterns in *pGL2-BRI1-GFP/bri1-T*.

(A) 7-day old WT, *bri1-T* and *pGL2-BRI1-GFP/bri1-T* roots grown under control conditions. Propidium iodide-staining is shown in grey and GFP in green. Scale bars, 100 μ m.

(B-C) UMAP projection of scRNA-seq from 14,334 wild-type cells, 12,649 *bri1-T* cells and 7,878 *pGL2-BRI1-GFP/bri1-T* cells. Two biological replicates of scRNA-seq were performed for each genotype. Colors indicate cell type annotation (B) or developmental stage (C).

(D) UMAP colored by DEGs for each cell type/developmental stage combination of *bri1-T* compared to WT.

(E) Volcano plot of DEGs in the elongating cortex from *bri1-T* compared to WT. Color indicates the direction of regulation.

(F-I) UMAP colored by DEGs for the indicated comparisons

(J) Multidimensional scaling (MDS) analysis of cortex cells from scRNA-seq. Note that replicates from the same genotype group together, but genotypes are well separated.

(K) Multidimensional scaling (MDS) analysis of atrichoblast cells from scRNA-seq.

(L-M) Gene expression trends for *bri1-T* vs wild-type DEGs along cortex (L) or atrichoblast (M) trajectories. Scaled expression along cortex pseudotime is plotted for each genotype. Lower bar indicates pseudotime progression calculated by CytoTRACE.

(Breuer et al., 2009, 2012) and root hairs (Shibata et al., 2018, 2021), but has not been linked to BR signaling or the cortex. Expression of *HAT7* and *GTL1* significantly increased in the cortex of our BRZ versus BL pseudobulk differential expression analysis at the 2 hour time point. On the other hand, although *JKD* was detected in WOT differential expression analysis, it did not pass our criteria for statistical significance in the 2 hour pseudobulk differential expression analysis (Data S3). Using a recombineering line (Moreno-Risueno et al., 2015), we found that *JKD* was present in the proliferation domain regardless of BRZ or BL treatment status and showed an increase in expression in the transition and elongation zone of the cortex upon BL treatment (Figures S3C and S3D). These results indicate that WOT trajectories can identify BR-responsive transcription factors that may be involved in regulating cell wall-related genes in the cortex.

To generalize our WOT analysis we constructed trajectories for each combination of cell type and developmental stage and performed differential expression analysis between each time point (Data S5). These data represent a valuable resource to generate additional hypotheses regarding spatiotemporal BR responses.

Analysis of the triple receptor mutant *bril-T* reveals changes in cortex expression

Since our results indicated that exogenous BRs lead to activation of cell wall-related genes in the elongating cortex, we asked if this is also the case for endogenous BRs. A gradient of BRs is present along the longitudinal axis of the root, with low BR levels in the proliferation domain (Vukašinović et al., 2021). BR biosynthesis increases as cells enter the transition domain and peaks in the elongation zone, shootward of which is a BR signaling maximum (Chaiwanon and Wang, 2015; Vukašinović et al., 2021). Interpretation of this endogenous BR gradient requires receptor *BRI1* and its close homologs *BRL1* and *BRL3* (Caño-Delgado et al., 2004; Friedrichsen et al., 2000; He et al., 2000; Irani et al., 2012; Kinoshita et al., 2005).

To identify differentially expressed genes, we performed two replicates of scRNA-seq on the BR-blind *bril1brl3* triple mutant (*bril-T*) along with paired wild-type controls (Figures 3A-C). A previous study profiled single cells from *bril-T* (Graeff et al., 2021), but these data were from a single replicate and were compared to a wild-type sample from a different study (Wendrich et al., 2020). Pseudobulk differential expression identified the elongating cortex as exhibiting substantial differential gene expression (Figures 3D-G, S4A and Data S3). The genes down-regulated in the elongating cortex of *bril-T* were enriched for the GO term “cell wall organization or biogenesis” (Figure S4B). These data indicate that, similar to exogenous application of BRs, endogenous BRs promote the expression of cell wall-related genes in the elongating cortex.

The epidermis is widely described as the major site for BR-promoted gene expression in the root (Chaiwanon and Wang, 2015; Fridman et al., 2014, 2021; Großholz et al., 2021; Hacham et al., 2011; Nolan et al., 2020; Vragović et al.,

2015; Wei and Li, 2016). Previous studies showed that epidermal expression of *BRI1* was sufficient to rescue morphological phenotypes including meristem size and root length of loss-of-function BR mutants such as *bril-T* (Fridman et al., 2014; Hacham et al., 2011; Kang et al., 2017). To determine the extent to which BR-regulated gene expression is restored, we performed scRNA-seq on *pGL2-BRI1-GFP/bril-T* - a line in which *BRI1* is expressed in atrichoblast cells of the epidermis of *bril-T* (Hacham et al., 2011; Kang et al., 2017; Vragović et al., 2015). We identified over 8,000 DEGs in comparison with wild type (Figures 3H and S4C-D) and in comparison with *bril-T* (Figures 3I and S4E-H), indicating that gene expression remains dramatically perturbed and that this is far from a complete rescue of the *bril-T* phenotype.

To further examine these gene expression changes, we aggregated cell-level counts for cortex cells and separately for atrichoblast cells of each sample and performed Multidimensional scaling (MDS) analysis. Samples of the same genotype appeared grouped across replicates for both cell types, but the *pGL2-BRI1-GFP/bril-T* replicates formed a distinct cluster from either wild-type or *bril-T* (Figure 3J).

Together, our scRNA-seq of BR treatment and *bril-T* indicate that the cortex represents a site of BR-mediated gene expression. The observation that *pGL2-BRI1-GFP/bril-T* has a distinct pattern of gene expression from WT or *bril-T* suggests that alternative means of probing tissue-specific BR responses could be informative.

Tissue-specific CRISPR of *BRI1* confirms a role for the cortex in BR-mediated cell expansion

To selectively block BR signaling in cell types of interest we performed tissue-specific CRISPR (Decaestecker et al., 2019) of *BRI1*. We used a *bril* mutant complemented with *pBRI1-BRI1-mCitrine* (Figure 4A) into which we introduced Cas9 driven by tissue-specific promoters to knock out *BRI1* either in the epidermis and lateral root cap (*pWER-BRI1-CRISPR*) or in the cortex (*pCO2-BRI1-CRISPR*). mCitrine signals were absent in the expected locations of the tissue-specific CRISPR lines, confirming their efficacy and specificity (Figures 4A-C and S5A-C).

Since our scRNA-seq data indicated that exogenous BRs promote the expression of cell wall-related genes in the elongating cortex, we hypothesized that loss of BR signaling in the cortex would affect final cell size. Indeed, *pCO2-BRI1-CRISPR* lines displayed significantly shorter mature cortex cells, while meristematic cortex cell length was relatively unaffected (Figures 4C-E).

In contrast, epidermal knockout of *BRI1* in *pWER-BRI1-CRISPR* lines resulted in both reduced meristem cell size and reduced mature cortex cell length (Figures 4C-E), which is consistent with the reported role of epidermal BR signaling (Chaiwanon and Wang, 2015; Fridman et al., 2021; Hacham et al., 2011; Vragović et al., 2015). These results indicate that in addition to the epidermis, BR signaling in the cortex is required to promote cell expansion in the elongation zone.

HAT7 and *GTL1* are BR responsive regulators along cor-

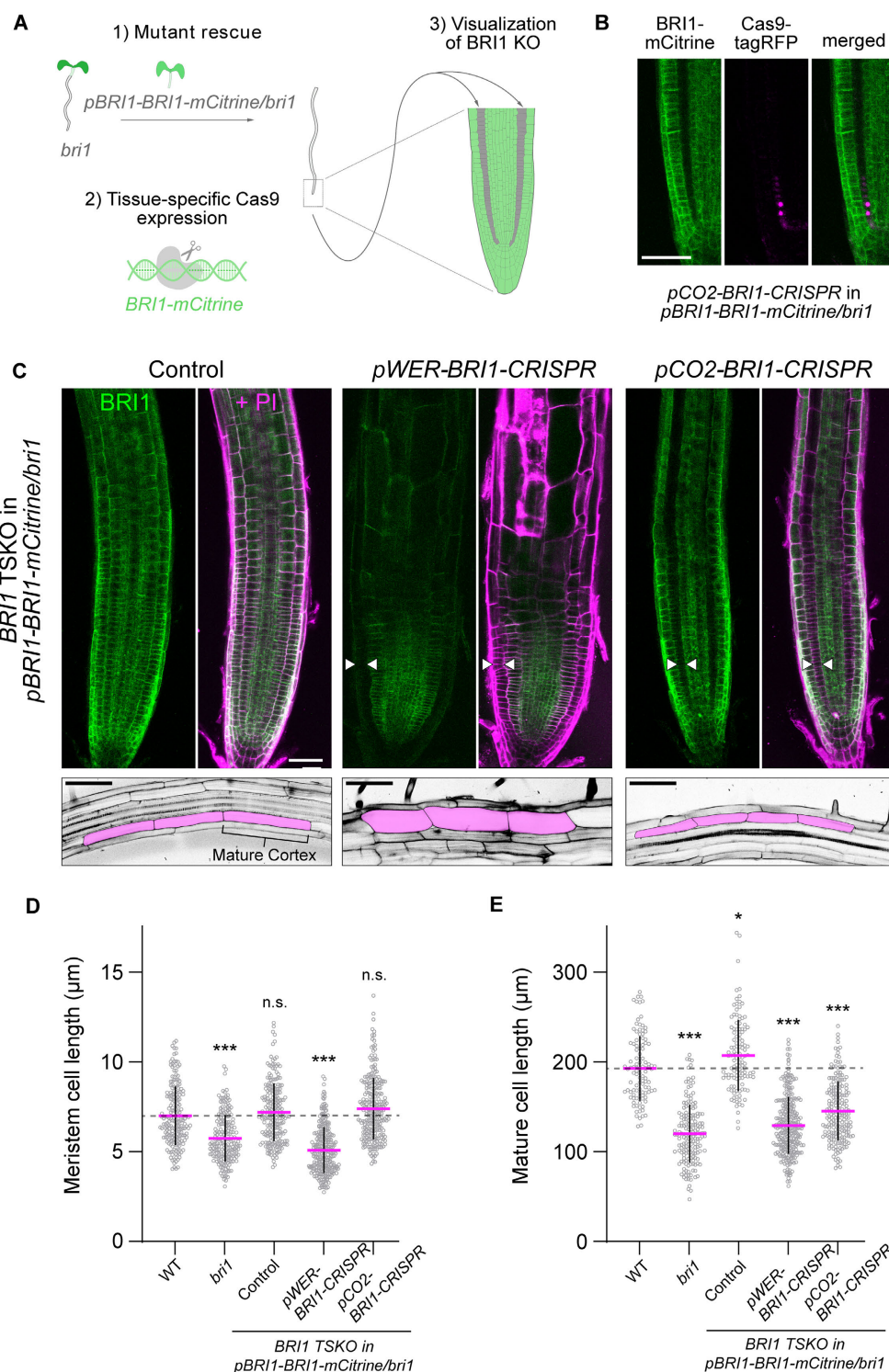


Fig. 4. Tissue-specific CRISPR of BRI1 confirms role for cortex in BR-mediated cell expansion.

(A) Overview of BRI1 tissue-specific CRISPR approach. A *bri1* mutant complemented with pBRI1-BRI1-mCitrine (1) was used as background to introduce tissue-specific Cas9 along with gRNAs targeting BRI1 (2). This allows for visualization of BRI1 knockout in specific cell layers, such as the cortex when pCO2-BRI1-CRISPR is used (3).

(B) Appearance of Cas9-tagRFP in the cortex is associated with loss of BRI1-mCitrine signal, confirming tissue-specific knockout.

(C) Confocal images of BRI1 tissue-specific CRISPR lines. Control indicates a broad expression pattern of BRI1-mCitrine in pBRI1-BRI1-mCitrine/*bri1*. BRI1-mCitrine signals are shown in green and propidium iodide staining (PI) in magenta (upper panels). White arrows specify tissues with absence of BRI1-mCitrine signal; epidermis for pWER-BRI1-CRISPR and cortex for pCO2-BRI1-CRISPR. Mature root sections illustrating changes in cell size and length (lower panels). Cortex cells are pseudocolored to indicate their position.

(D) Quantification of meristematic cortex cell length, defined as the first 20 cells of individual roots starting from the quiescent center. Control indicates pBRI1-BRI1-mCitrine/*bri1* complemented line.

(E) Quantification of mature cortex cell length. For (D) and (E), all individual data points are plotted. Magenta horizontal bars represent the means and error bars represent s.d. Significant differences between each line and wild type were determined by one-way ANOVA and Dunnett's multiple comparison tests. *** $P < 0.001$, ** $P < 0.01$ and * $P < 0.05$. n.s. not significant. Scale bars, for (B) and (C) = 50 μm. TSKO, tissue-specific knockout.

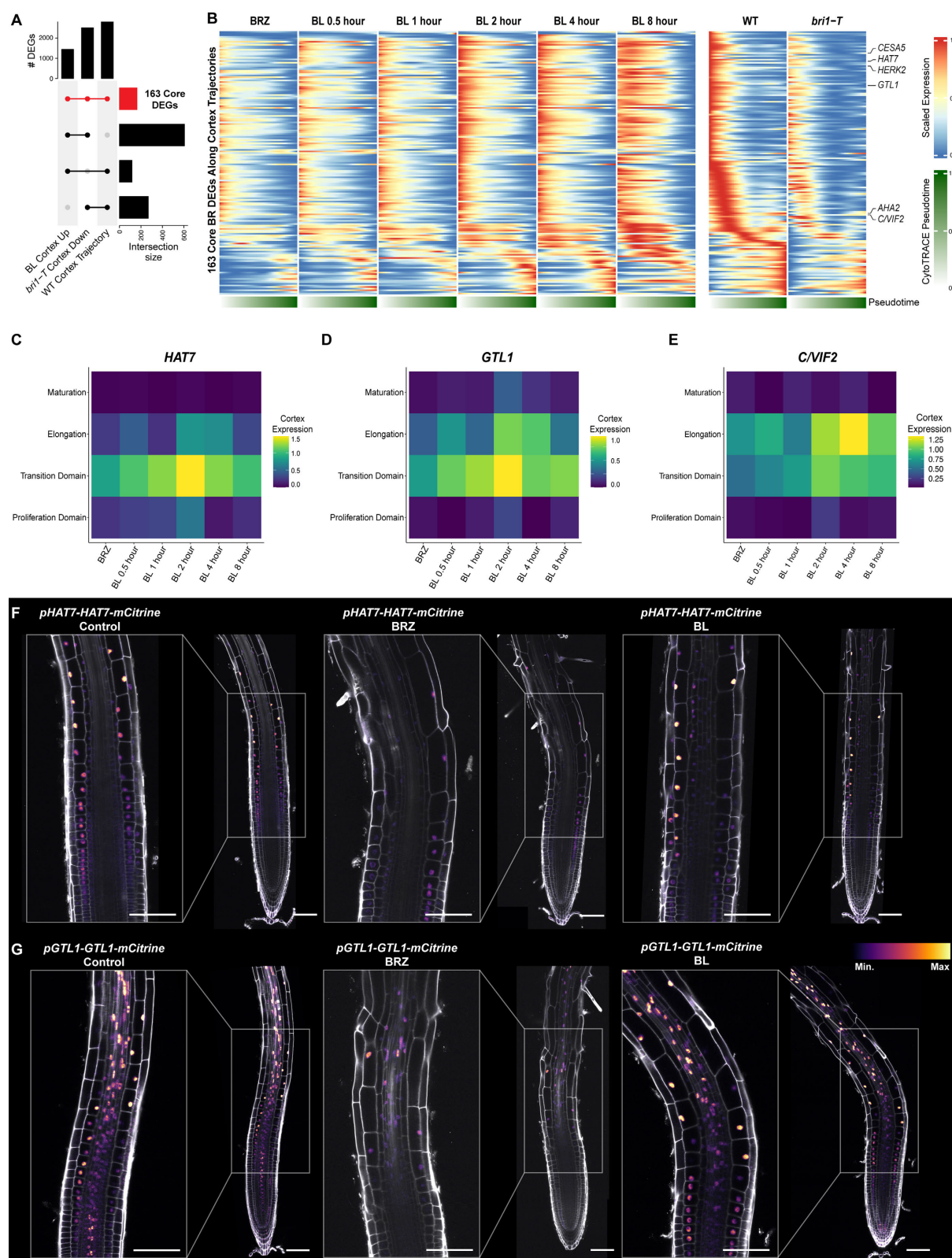


Fig. 5. *HAT7* and *GTL1* are BR responsive regulators along cortex trajectories.

(A) Upset plot showing a comparison of genes up-regulated by BL in the cortex, down-regulated in the cortex of *bri1-T*, and differentially expressed along wild-type cortex trajectories. Red color indicates 163 genes common to all three sets.

(B) Gene expression trends for 163 core BR DEGs along cortex trajectories. Scaled expression along cortex pseudotime is plotted for each time point of the BR time series and for wild type versus *bri1-T*. Lower bar indicates pseudotime progression calculated by CytoTRACE.

(C-E) Gene expression trends for *HAT7*, *GTL1* or *C/VIF2* along the developmental zones of the cortex (y-axis) for each time point of the BR time course (x-axis). Color bar indicates the scaled expression level in the cortex.

(F-G) 7-day old roots expressing *pHAT7-HAT7-mCitrine* or *pGTL1-GTL1-mCitrine* reporters under the indicated treatments. Control represents a mock DMSO solvent. For BRZ and BL treatments, plants were grown on 1 μ M BRZ for 7 days and transferred to 1 μ M BRZ or 100nM BL for 4 hours. Propidium iodide-staining is shown in grey, with the color gradient indicating relative mCitrine levels. Scale bars, 100 μ m. BL, brassinolide; BRZ, brassinazole.

tex trajectories

To define a core set of genes associated with BR response along cortex trajectories we first compared genes induced in the cortex by BL treatment with those down-regulated in the cortex of *bril-T*. Of the 768 genes in common, we then asked which vary along developmental time in wild-type cortex trajectories (Shahan, Hsu et al 2022). The intersection of these three lists identified a core set of 163 BR responsive DEGs (Figure 5A and Data S3). Consistent with regulation by BRs, 69% of the core DEGs are BES1 and BZR1 direct targets from ChIP experiments (Oh et al., 2014; Sun et al., 2010; Yu et al., 2011). Expression along cortex pseudotime illustrates induction by BL treatment and down-regulation in *bril-T* (Figure 5B). Additionally, *HAT7* and *GTL1* were induced along these trajectories, suggesting a potential role for these transcription factors in controlling BR-regulated gene expression in the cortex (Figure 5C-E and S6A).

To gain insight into their roles, we generated translational reporter lines for *HAT7* and *GTL1* and monitored their expression. Under control conditions, *pHAT7-HAT7-mCitrine* lines showed expression in the transition domain and elongation zone of the cortex (Figure 5F), consistent with previous reports (Lee et al., 2006). We also observed *HAT7* signals in the epidermis and endodermis, in line with expression patterns in our wild-type scRNA-seq atlas (Shahan et al., 2022). *HAT7* expression was decreased when BR biosynthesis was inhibited with BRZ, and restored upon BL treatment (Figures 5F and S6A).

pGTL1-GTL1-mCitrine was more broadly expressed, with increasing levels in the cortex and epidermis as cells progress from the transition domain to the elongation zone (Figures 5G and S6A). *GTL1-mCitrine* expression was reduced by BRZ and increased by BL treatment (Figure 5G). These results confirm that BRs promote the expression of *HAT7* and *GTL1* coinciding with the onset of cell elongation. Furthermore, *HAT7* and *GTL1* are direct targets of BES1 and BZR1 (Oh et al., 2014; Sun et al., 2010; Yu et al., 2011), suggesting that they may be part of the BR-directed GRN activated as cells progress from proliferation to elongation.

Previous studies have inferred global (Guo et al., 2013; Seyed Rahmani et al., 2021; Sun et al., 2010; Xie et al., 2019a; Yu et al., 2011) or temporally resolved GRNs (Clark et al., 2021) for BR response, but they lack cell type and developmental-stage specificity. To infer GRN configurations across our BR time series we used CellOracle (see methods; Data S8) focusing on BL DEGs and associated transcription factors.

Analysis of network importance scores such as centrality measures is a powerful approach to prioritize candidate regulators among DEGs (Iacono et al., 2019; Kamimoto et al., 2020). Since the cell wall signature peaked at 2 hours after BL treatment, we prioritized transcription factors with high network centrality scores in the elongating cortex at this time point. *HAT7* was the top-ranked transcription factor in terms of degree centrality and three close homologs: *HB13*, *HB20* and *HB23* were also among the top 10 transcription factors (Figures 6A-B and Data S8). Together *HAT7*, *HB13*, *HB20* and *HB23* make up the alpha clade HD-ZIP I transcription

factors in Arabidopsis (Ariel et al., 2007; Henriksson et al., 2005; Mattsson et al., 1992). Genetic analysis of *HAT7* has yet to be carried out, but *HB13*, *HB20* and *HB23* have been implicated in root development (Perotti et al., 2019; Silva et al., 2016), shoot development (Ribone et al., 2015), and stress responses (Ebrahimian-Motlagh et al., 2017; Gao et al., 2014; Harris et al., 2011; Perotti et al., 2021).

We used CRISPR to generate *hat7* loss-of-function mutants but did not observe strong phenotypes in terms of cortex cell elongation (Figure S6D-F). Since *HB13*, *HB20* and *HB23* are induced by BRs and predicted to regulate cell wall-related genes in our GRNs (Figures 6B, S6A-B and Data S10), we next generated *hat7 hb13 hb20 hb23* quadruple mutants via multiplex CRISPR (Stuttman et al., 2021). Mature cortex cell length was reduced by approximately 25% in two independent quadruple mutants (Figures 6C-E and S6E), providing strong evidence that *HAT7* and its homologs are required for cell elongation. Despite the decrease in final cell length, the root length of the quadruple mutant was not dramatically reduced (Figure S5D), suggesting that the decrease in cell length is at least partially compensated for by increased cell production.

We next investigated *GTL1*, which was the 5th highest ranked TF in the BL 2 hour elongating cortex GRN in terms of degree centrality (Figures 6A-B). Given that *GTL1* was shown to function redundantly with its close homolog *DF1* in terminating root hair growth (Shibata et al., 2018, 2021), we examined *gtl1* and *df1* single mutants along with *gtl1 df1* double mutants. *gtl1* and *df1* displayed only subtle changes in mature cortex cell length. However, *gtl1 df1* double mutant had significantly shorter mature cortex cell lengths and shorter roots (Figures 6C-E and S6D-F). As previously reported (Shibata et al., 2018), *DF1* was expressed at lower levels as compared to *GTL1*, making *DF1* challenging to detect in scRNA-seq (Figure S6A-B). Despite this, we observed increasing trends of *DF1* expression along WOT trajectories in the BL time course, especially in cortex cell wall+ cells (Figure S6B). We also verified that BL treatment results in an increase in *pDF1-DF1-GFP* levels as compared to BRZ controls (Figure S6C). Together, our genetic analysis of *HAT7* and *GTL1* family transcription factors illustrates the power of GRN-mediated discovery of regulatory factors in spatiotemporal BR response.

BES1 and GTL1 physically interact and share a common set of target genes

Since BES1 is known to interface with other transcription factors in controlling BR-regulated gene expression, we compared target genes for BES1 and BZR1 (Oh et al., 2014; Sun et al., 2010; Yu et al., 2011) to ChIP targets of *GTL1* and *DF1* (Shibata et al., 2018). BES1 and BZR1 share 3,020 common targets with *GTL1*, significantly more than expected by chance (Figure S7A, $P < 0.001$, Fisher's exact test). Similarly, BES1 and BZR1 share 2,490 common targets with *DF1* (Figure S7A, $P < 0.001$, Fisher's exact test). When compared to BR-regulated genes from scRNA-seq, BES1 and *GTL1* targets showed the strongest enrichment in genes up-

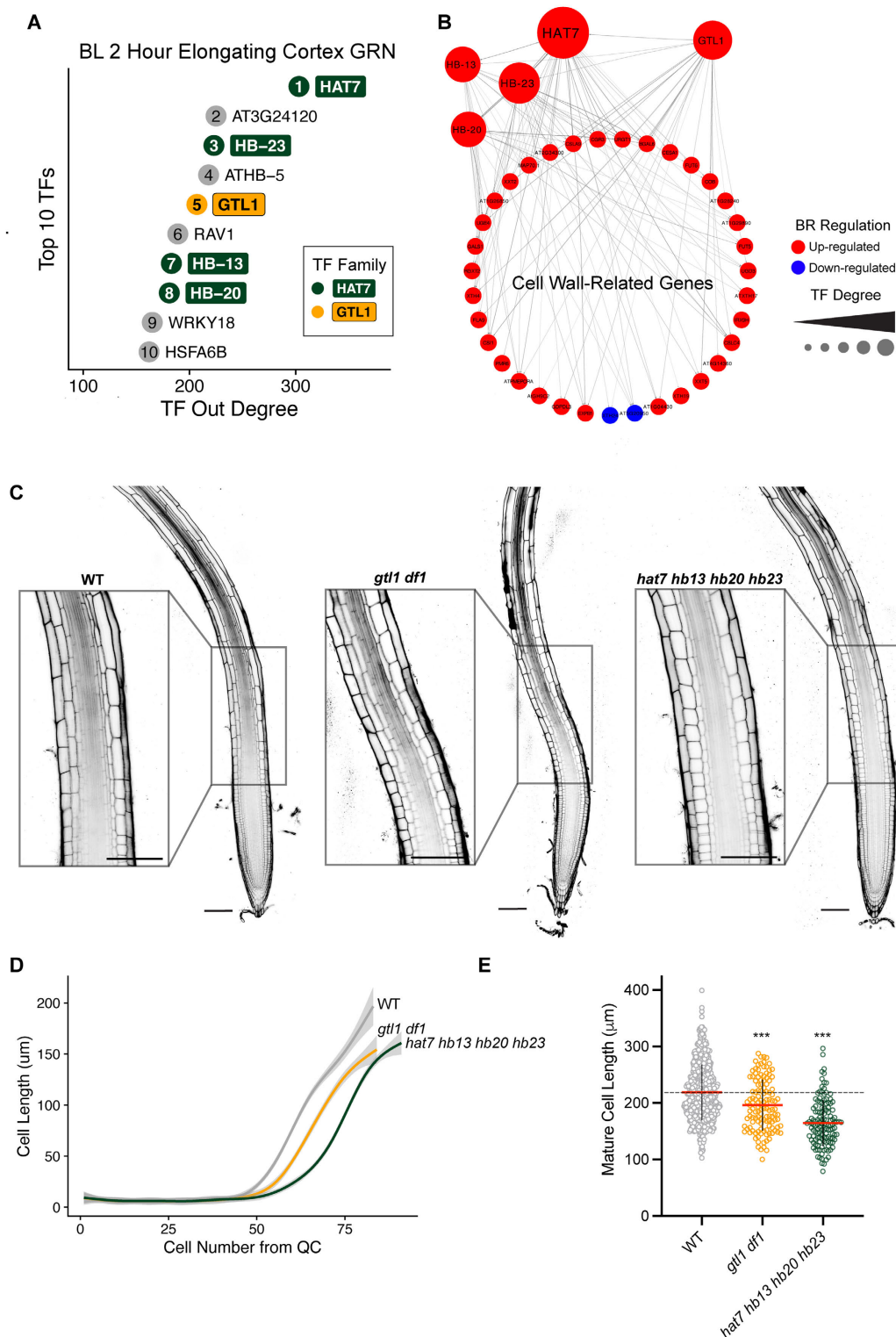


Fig. 6. HAT7 and GTL1 are top-ranked regulators in cortex GRNs and affect BR-related phenotypes.

(A) Top 10 transcription factors (TFs) in the CellOracle BL two-hour elongating cortex GRN ranked by out degree. The ranking is indicated by the number inside the circle. Color indicates TF family, with light grey corresponding to any family other than HAT7 or GTL1.

(B) Subnetwork showing cell wall-related genes that are predicted targets of HAT7 and GTL1 in the CellOracle elongating cortex GRN. HB13, HB20 and HB23 are included in the subnetwork since they are connected to HAT7 and cell-wall-related genes.

(C) Propidium iodide-staining of 7-day-old WT, *hat7 hb13 hb20 hb23* (line 1-2), and *gtl1 df1* roots. Insets show cortex cells entering the elongation zone. Scale bars, 100 μm.

(D) Quantification of cortex cell length along the longitudinal axis of the root. The quiescent center was designated as "0" and each cell number consecutively thereafter. The grey area represents the confidence interval of the smoothed mean estimated with a generalized additive model. Number of roots per genotype: WT=51, *gtl1 df1*=26, *hat7 hb13 hb20 hb23*=16.

(E) Quantification of mature cortex cell length. Red horizontal bars represent the means and error bars represent s.d. Significant differences between each line and wild type were determined by one-way ANOVA and Dunnett's multiple comparison tests. ***P<0.001.

regulated by BRs in the transition domain and elongation zone of the cortex (Figure S7B), with 297 common targets of both BES1 or BZR1 and GTL1 being induced in the elongating cortex by BL treatment.

Given the strong overlap between BES1 and GTL1 targets, we hypothesized that these TFs physically interact to regulate a common set of genes. Co-immunoprecipitation showed that GTL1-FLAG pulled down BES1-GFP (Figure S7C). These results suggest that BRs induce GTL1 and subsequently BES1 and GTL1 interact to control a common set of target genes.

scRNA-seq reveals cell-type-specific expression underlying *gtl1 df1* phenotypes

Our results indicate that *gtl1 df1* mutants have reduced cortex cell elongation. On the other hand, *gtl1 df1* mutants have longer trichoblasts or root hairs (Shibata et al., 2018). A downstream regulatory network that enables GTL1-mediated growth inhibition has been dissected in trichoblasts (Shibata et al., 2018). To identify the cell-type-specific changes in gene expression underlying *gtl1 df1* cortex phenotypes we performed scRNA-seq on *gtl1* and *df1* single mutants, and on the *gtl1 df1* double mutant. Using pseudobulk differential expression analysis, we detected relatively subtle changes in *gtl1* or *df1* single mutants compared to wild type (Figures 7A-B). In contrast, over 8,000 genes were differentially expressed in *gtl1 df1* double mutants versus wildtype (Figure 7C).

Over 1,000 genes were up-regulated across all developmental stages of the cortex of *gtl1 df1*, and an approximately equal number of genes were down-regulated. The majority of cortex DEGs were affected in the elongation zone (Figures 7D-E, S7D and Data S3). Of the down-regulated genes in the cortex of the double mutant, 226 genes were also up-regulated by BL treatment. Furthermore, 31.3% of the core BR DEGs were down-regulated in the cortex of *gtl1 df1*, whereas only 6.8% were up-regulated (Data S3). The larger proportion of genes up-regulated by BRs but down-regulated in the cortex of *gtl1 df1* suggests that GTL1 and DF1 promote the expression of a subset of BR-induced genes in the cortex.

Plotting *gtl1 df1* DEGs along cortex pseudotime illustrated the down-regulation of several genes involved in cell elongation including CESA5 and AHA2 (Figure 7E). These genes were significantly enriched for the GO term “cell wall organization or biogenesis” (Figure S7E). We next examined *C/VIF2*, because it is induced by BL in the cortex (Figures 1G-H), but its expression decreased in cortex cells of *gtl1 df1* (Figures 7F-G). A *pC/VIF2-H2B-Venus* reporter showed expression of *C/VIF2* in the transition and elongation zone of the wild-type cortex, whereas its expression was reduced in the cortex of *gtl1 df1* mutants (Figure 7H and Video S1).

Taken together, our results establish the elongating cortex as a site of BR-regulated expression associated with cell elongation. Reconstruction of cortex trajectories revealed BR induction of cell wall-related genes that coincide with the switch to elongation and identified HAT7 and GTL1 as BR-responsive regulators of cortex GRNs. The reduced expression of cell

wall-related genes in *gtl1 df1* mutants validates our cell-type-specific BR GRNs and identifies a function of GTL1 in promoting cortex cell elongation in response to BRs.

Discussion

Understanding how hormone-mediated GRNs are controlled in space and time has the potential to enable the engineering of specific downstream responses to optimize plant growth under a changing environment (Fàbregas et al., 2018; Gupta et al., 2020; Nolan et al., 2020). Plant hormones including BRs, auxin, gibberellins, and abscisic acid have been shown to exhibit tissue-specific responses (Ackerman-Lavert and Savaldi-Goldstein, 2020; Bargmann et al., 2013; Geng et al., 2013; Iyer-Pascuzzi et al., 2011; Shani et al., 2013; Ubeda-Tomás et al., 2008, 2009), but how the associated GRNs are modulated in different cell types at particular developmental stages is largely enigmatic. In this study, we profiled BR-responses across cell types, developmental stages and time points of treatment using scRNA-seq, providing a high-resolution map of signaling outputs. We identified the elongating cortex as a spatiotemporal context for BR signaling, where BRs activate cell wall-related genes and promote elongation. We further showed that HAT7 and GTL1 are BR-induced regulators along cortex trajectories that control cell elongation. Our findings reveal spatiotemporal BR responses and the underlying GRNs at unprecedented resolution.

BR signaling is arguably one of the best-characterized signaling pathways in plants (Nolan et al., 2020; Planas-Riverola et al., 2019) and there is considerable evidence for tissue-specific BR responses, especially in roots (Ackerman-Lavert and Savaldi-Goldstein, 2020; Fridman et al., 2021; Graeff et al., 2021; Jaillais and Vert, 2016; Vukašinović et al., 2021). Despite these efforts, characterization of cell-type-specific BR signaling has relied on tissue-specific complementation lines, which have led to conflicting results and have not examined the role of BR signaling in the cortex (Chaiwanon and Wang, 2015; Fridman et al., 2014; Graeff et al., 2020, 2021; Hacham et al., 2011; Kang et al., 2017; Pavelescu et al., 2018; Vragović et al., 2015).

Epidermal expression of the BR receptor BRI1, as well as downstream transcription factor BZR1, have been shown to partially rescue root morphology defects of BR signaling mutants (Chaiwanon and Wang, 2015; Fridman et al., 2014; Hacham et al., 2011; Vragović et al., 2015). On the other hand, BRI1, but not BES1 or BZR1, was reported to rescue *bri1-T* morphology when expressed in the developing phloem using the *CVP2* promoter (Graeff et al., 2020; Kang et al., 2017), likely through non-canonical signaling factors operating downstream of BRI1. Importantly, gene expression was not fully restored to wild-type levels in either epidermal or phloem rescue lines. Our scRNA-seq of epidermal *pGL2-BRI1-GFP/bri1-T* lines showed patterns of gene expression distinct from either wild type or *bri1-T*. Similarly, scRNA-seq of *pCVP2-BRI1-CITRINE/bri1-T* indicated an intermediate state between wild type and *bri1-T* (Graeff et al., 2021). These observations along with our finding that BRs influence gene expression in the elongating cortex motivated us to dis-

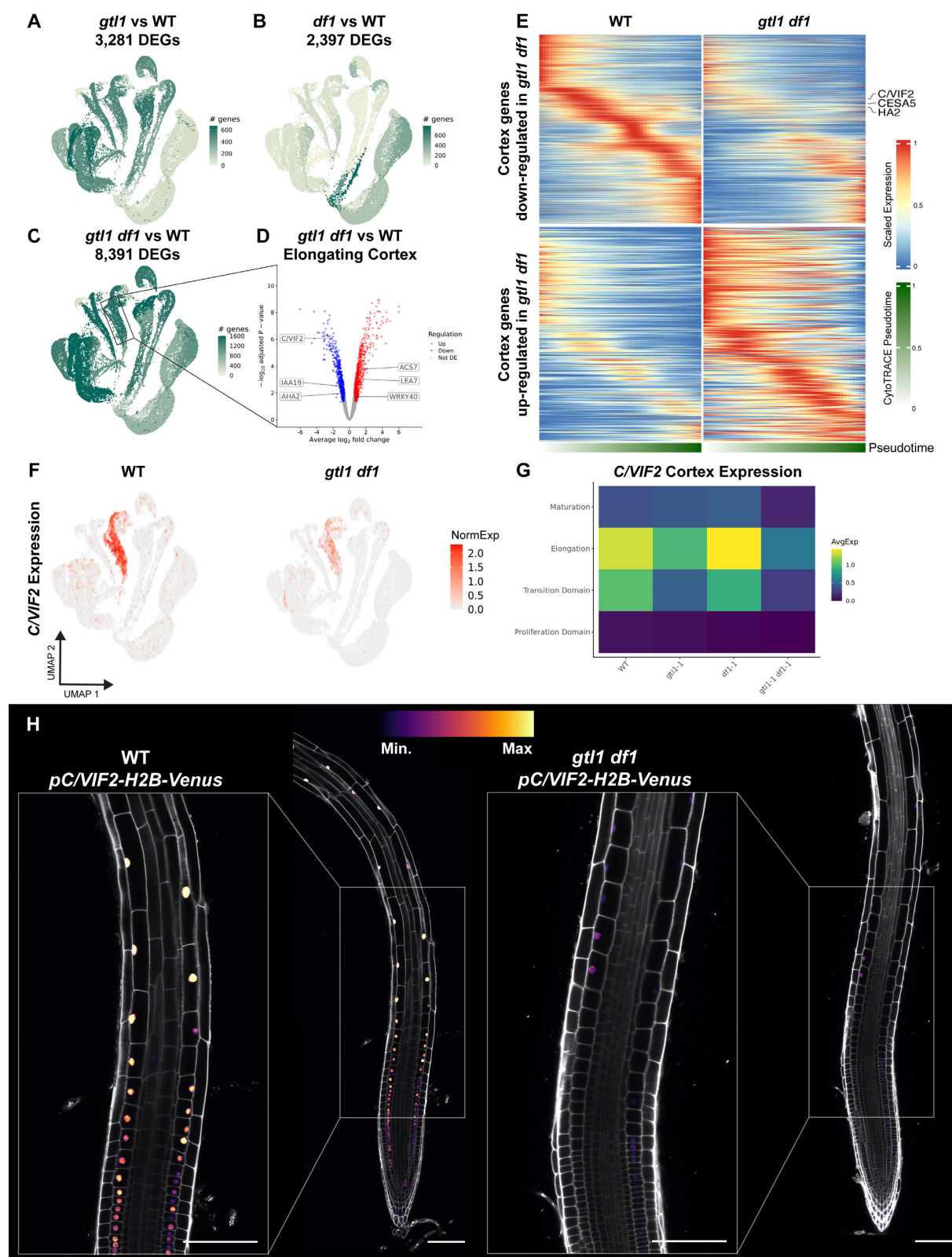


Fig. 7. scRNA-seq reveals cell-type-specific expression underlying *gtl1 df1* phenotypes

(A-C) UMAP projection of scRNA-seq from 74,810 WT, *gtl1*, *df1*, and *gtl1 df1* cells. Two biological replicates were profiled for each genotype. Color indicates DEGs for each cell type/developmental stage combination of *gtl1* compared to WT (A), *df1* compared to WT (B) or *gtl1 df1* compared to WT (C).

(D) Volcano plot of DEGs in the elongating cortex from *gtl1 df1* compared to WT. Color indicates the direction of regulation.

(E) Gene expression trends along cortex trajectories for DEGs in *gtl1 df1* compared to WT. Each row represents the scaled expression of a gene along cortex pseudotime. The lower bar indicates pseudotime progression calculated by CytoTRACE.

(F) Expression of *C/VIF2* in wild type and *gtl1 df1* scRNA-seq. The color scale represents log normalized, corrected UMI counts.

(G) Gene expression trends plotted along developmental zones of the cortex (y-axis) for WT, *gtl1*, *df1*, and *gtl1 df1*. The color bar indicates the scaled expression level.

(H) 7-day old root images of a *pC/VIF2-H2B-Venus* reporter in wild type or *gtl1 df1* under control conditions. Propidium iodide-staining is shown in grey, with the color gradient indicating relative mCitrine levels. Scale bars, 100 μ m.

sect cell-type-specific BR phenotypes.

Using tissue-specific CRISPR we found that the phenotype associated with loss of *BRI1* depends on the cell type. Tissue-specific knockout of *BRI1* in the cortex reduced final cell size, but did not markedly influence the meristem. This is consistent with the idea that BRs induce the expression of cell wall-related genes in the elongating cortex to promote cell expansion. In contrast, scRNA-seq showed that BRs affect gene expression more broadly across the developmental zones of the epidermis. Accordingly, we observed both meristem cell length and final cell size were reduced when *BRI1* was knocked out in the epidermis and LRC. It has been suggested that the cortex could instruct anisotropic growth through its physical connection with the epidermis, but as the outermost tissue, relaxation of the epidermis is required to allow for cell elongation (Baskin and Jensen; Bou Daher et al., 2018). This may explain the apparent widening of cortex cells in pWER-*BRI1*-CRISPR lines. It is plausible that continued BR signaling in the cortex promotes expansion which is physically limited by the stiff outer epidermal cells that lack BR signaling in pWER-*BRI1*-CRISPR roots. Future studies could examine how cell elongation is coordinated between these neighboring tissues in the *BRI1* tissue-specific CRISPR lines.

Notably, *BRI1* driven by its native promoter was still present in the stele of our tissue-specific CRISPR lines when we observed these phenotypic defects, suggesting that, unlike *pCVP2-BRI1*, native expression of *BRI1* in the stele is not sufficient for BR-induced cell elongation and root growth. These results confirm the role of the epidermis in BR-regulated root growth and reveal the function of cortex in BR-mediated cell expansion, demonstrating how scRNA-seq can identify a new spatiotemporal context for hormone signaling.

Our findings also highlight the ability of single-cell genomics to identify context-specific transcription factors, a capability that could be leveraged to precisely engineer plant growth, development, and/or responses to stress. Multiple lines of evidence suggest that HAT7 and GTL1 are BR-responsive regulators along cortex trajectories. HAT7 and GTL1 expression increased in exceptionally responsive cortex cell wall + cells along WOT trajectories. This suggests that HAT7 and GTL1 are associated with high relative expression of BR-induced cell wall-related genes and promote the shift from transition domain to elongation zone. We also found that HAT7 and GTL1 were among a core set of BR-responsive genes along cortex trajectories and are induced by BR treatment but decreased in *bri1-T*. Examination of HAT7 and GTL1 reporters supported these observations, showing that HAT7 and GTL1 are induced by BRs and increase in expression as cortex cells elongate. HAT7, GTL1, and several close homologs were among the top 10 ranked transcription factors in elongating cortex GRNs. We showed that *hat7 hb13 hb20 hb23* quadruple mutants and *gtl1 dfl* double mutants have reduced mature cortex cell lengths. However, neither of these multiple mutants had a phenotype as severe as complete loss-of-function mutants in the pathway such as *bri1-T*. Considering that most gene promoters are controlled by multiple transcription fac-

tors, it's likely that additional transcription factors cooperate with GTL1 and/or HAT7 in the regulation of genes involved in cell elongation in the cortex. Advances such as combinatorial CRISPR screens (Gaillochet et al., 2020) pave the way to investigate potential genetic redundancy between HAT7, GTL1, and other regulatory factors identified in our cortex GRNs.

A common theme in BR signaling networks is that BES1 and BZR1 bind to the promoters of downstream transcription factors to control their expression and then subsequently physically interact with these transcription factors to co-regulate target genes (Guo et al., 2013; Li et al., 2009; Nolan et al., 2020; Ye et al., 2017). This type of feed-forward loop could provide a mechanism to amplify the BR signal and/or to direct BES1, a more broadly expressed transcription factor, to drive tissue-specific gene expression by interacting with other more specifically expressed transcription factors. Our findings reinforce this theme and also add spatiotemporal context to such networks. GTL1 is a direct ChIP target of BES1 and BZR1 (Oh et al., 2014; Sun et al., 2010; Yu et al., 2011) and is induced by BRs. BES1 and GTL1 physically interact and share over three thousand common target genes, with the strongest enrichment among genes up-regulated by BRs in the transition and elongation zones of the cortex. Our scRNA-seq analysis showed a corresponding reduction of BR-induced genes in the cortex of *gtl1 dfl*, supporting the hypothesis that GTL1 is required for BR-regulated gene expression and cortex cell elongation.

Although we focused on BR control of cell elongation in the cortex in this study, many additional aspects of spatiotemporal BR responses remain to be explored. Our data represent a rich resource to investigate BR-induced changes in cell identity as has been shown for trichoblasts versus atrichoblasts in the epidermis (Cheng et al., 2014; Kuppasamy et al., 2009). Comparison of BR treatment versus mutant datasets could provide insight into the maintenance of procambium identity in the stele, which requires *BRI1* in a BR-independent manner (Holzwardt et al., 2018). Our BR GRNs could also be used to dissect the transcriptional responses in other contexts such as the meristem, where a dual function of BRs in promoting auxin levels but inhibiting auxin signaling operates through unknown regulators in the epidermis (Ackerman-Lavert et al., 2021). To facilitate such discoveries, we have made our data publicly available as an interactive browser <https://shiny.mdc-berlin.de/ARVEX/> which allows users to query gene expression patterns, DEG tables, WOT results and CellOracle GRNs.

In summary, our scRNA-seq analysis and tissue-specific gene manipulations demonstrated that the cortex is involved in BR-regulation of cell wall-related genes and cell elongation. We further identified HAT7, GTL1 and their homologs as critical regulators that cooperate with BES1 to drive cortex-specific gene expression and the transition to cell elongation in response to BRs. This study provides a rich resource to identify additional regulators that dictate BR actions in the cortex and other tissues in a precise spatiotemporal manner.

Methods

Plant materials and growth conditions

Arabidopsis accession Columbia-0 (Col-0) was used as a wild type. The following lines were previously described: *bri1 GABI_134E10* (Jaillais et al., 2011); *bri1-116bri1bri3* triple mutant (*bri1-T*) (Irani et al., 2012); *pGL2-BRI1-GFP/bri1-T* (Vragović et al., 2015); *gtl1-1* (WiscDsLox413-416C9), *df1-1* (SALK_106258), and *gtl1-1 df1-1* (Shibata et al., 2018); JKD-Ypet recombineering line (Moreno-Risueno et al., 2015). Seeds were sterilized using 50% (v/v) bleach with 0.05% Tween-20 for 10-15 minutes, plated on 1/2 Linsmaier and Skoog (LSP03-1LT, Caisson Labs; pH 5.7), 1% sucrose media, and stratified 2-4 days at 4°C in the dark. Plates were kept vertically in a Percival growth chamber set to 22°C, 16 hours light/8 hours dark and grown for 7 days unless otherwise indicated. Chemical treatments were conducted by cooling the growth media to approximately 60°C after autoclaving and adding DMSO (a mock solvent), 1 µM Brassinazole (BRZ, SML1406, Sigma) or 100nM Brassinolide (BL, 21594, Cayman Chemical).

bri1-T was maintained as a heterozygote for *bri1-116* and homozygous mutants were confirmed as previously described (Kang et al., 2017). Primers listed in Data S11 were used to amplify genomic DNA and the resulting 552bp amplicon was digested with *PmeI*. The mutant *bri1-116* allele could not be digested, whereas WT was cut into 314bp and 238bp fragments.

Transgenic reporters

To generate new reporters for BR-responsive genes, we first added the FASTRED seed coat selection cassette (Shimada et al., 2010; Stuttmann et al., 2021) and a MoClo (Engler et al., 2014) Level 1 acceptor site to the binary vector pICH86966 (Addgene plasmid #48075). *pHAT7-HAT7-mCitrine* and *pGTL1-GTL1-mCitrine* were assembled into this FASTRED destination vector using Level 1 BsaI golden gate assembly. To facilitate one-step promoter-reporter construction, we assembled an AarI flanked RFP dropout using the overhangs described in the Mobius (Andreou and Nakayama, 2018) upstream of Venus-H2B followed by the Ubiquitin10 terminator (tUBQ10), a plasma membrane marker (pUBQ10-mScarlet-LTI6-tNos), and a constitutive histone maker (pUBQ10-H2B-CFP-t19s). Promoters containing up to ~3kb of sequence upstream of the ATG start codon for the gene of interest were PCR amplified with AarI containing primers and used to replace the AarI-RFP module in golden gate reactions to generate Promoter-Venus-H2B constructs. Our Venus-H2B reporter included a Ubiquitin tag to decrease reporter perdurance. Although the plasma membrane marker and histone marker were included as positive controls in the constructs, they were not further analyzed in this study.

Assemblies were confirmed by restriction digestion and sequencing, transformed into *Agrobacterium*, and used to transform Arabidopsis via floral dip (Clough and Bent, 1998). FASTRED positive T1 seeds were selected under a fluorescent dissecting scope and only lines with 3:1 segregation of seed coat fluorescence in the T2 generation were

used. T2 lines with bright seed fluorescence were typically homozygous in our conditions. Therefore, we used bright T2 seeds or homozygous T3 seeds for experiments. We ensured that reporter signals were consistent across at least three independent transgenic lines.

Generation of mutant lines using multiplex CRISPR

We produced *hat7* single mutants and *hat7 hb13 hb20 hb23* quadruple mutants using FASTRED multiplex CRISPR constructs containing an intronized version of Cas9 (Grützner et al., 2021; Stuttmann et al., 2021). Two gRNAs were designed per gene using CHOP-CHOP (Labun et al., 2019). gRNA containing oligos were hybridized and cloned into pDGE sgRNA shuttle vectors using *BpiI* (Data S11). Each of the gRNA containing shuttle vectors were then assembled into pDGE666 (Addgene plasmid # 153231) using BsaI golden gate assembly, sequence verified, and transformed into wild-type Arabidopsis as described above. We selected FASTRED positive T1 seeds and subsequently screened FASTRED negative (putatively Cas9-free) T2 seeds for frameshift mutations using Sanger sequencing coupled with ICE analysis of CRISPR edits (Conant et al., 2022). The edits were similarly confirmed in the T3 generation and at least two homozygous alleles from independent lines were used for experiments.

BRI1 tissue-specific CRISPR

Two gRNA-BRI1 were simultaneously expressed in a tissue-specific manner (Decaestecker et al., 2019). Primers used for cloning of gRNA BRI1-2 (Feng et al., 2013) and gRNA BRI1-3 can be found in Data S11. The entry module pGG-B-AtU6-26-BRI1-2-C and pGG-A-AtU6-26-BRI1-3-B were generated by annealing oligos for each gRNA and ligating into *BbsI*-digested (New England Biolabs) Golden Gate entry vectors described in (Houbaert et al., 2018). Next, gRNA modules were combined with pGG-C-linker-G plasmid and cloned into pEN-R2-A-G-L3 by restriction-ligation using BsaI enzyme (New England Biolabs) to obtain pEN-R2- gRNA_BRI1-3-gRNA_BRI1-2-L3. This plasmid was combined with pDONR-L1-Cas9p-tagRFP-L2 (Wang et al., 2020), pDONRL4-L1r carrying either WER or CO2 promoters (Marquès-Bueno et al., 2016) and a destination vector pK8m34GW-FAST (Vanholme et al., 2013) in a MultiSite Gateway LR reaction (Thermo Fisher Scientific) to obtain expression clones. Expression clones were introduced into *Agrobacterium* C58 strain and used to transform *pBRI1-BRI1-mCitrine/bri1* plants (Jaillais et al., 2011) by floral dip. T2 generation seeds were selected based on the presence of GFP signal in the seed coat and 7-day-old seedlings were used for phenotypic analysis. For each root used for quantitative analysis, BRI1-mCitrine signal was acquired in order to confirm efficiency of the tissue-specific knockout system. Statistical analyses were conducted in GraphPad Prism v.9 software.

Confocal microscopy

Confocal imaging for the majority of experiments was per-

formed using a Zeiss 880 equipped with a 40X objective. Excitation and detection were set as follows: Venus and mCitrine, excitation at 488 nm and detection at 499–571 nm; GFP, excitation at 488 nm and detection at 493–558 nm; PI staining, excitation at 561 nm and detection at 605–695 nm. Confocal images were processed using the Fiji package of ImageJ (Schindelin et al., 2012). Tile scans were stitched and representative median longitudinal sections for each image are shown. Identical settings were used for images that were directly compared.

For BRI1 TSKO confocal, roots were imaged between a block of agar and cover glass in imaging chambers. Image acquisition was performed with a FluoView1000 inverted confocal microscope (Olympus) equipped with a dry 20X objective (NA 0.75) using 514 nm laser excitation and a spectral detection bandwidth of 500–530 nm for mCitrine and 535 nm laser excitation together with a spectral detection bandwidth of 570–670 nm for PI.

For the confocal time-lapse video, 7-day-old wild type and *gtl1 dfl* seedlings expressing *pC/VIF2-H2B-VENUS* were placed on ½ MS agar blocks containing PI, placed side-by-side in chambered coverglass (Nunc Lab-Tek, ThermoFisher) and imaged under a vertical ZEISS LSM900 microscope equipped with a Plan-Apochromat M27 20x/0.8 n.a. objective. The root tip was imaged every 12 min and automatically tracked with the TipTracker software (von Wangenheim et al., 2017). The excitation/emission wavelengths were 514 nm/530–600 nm for Venus and 535 nm/580–650nm for PI.

BES1 and GTL1 Co-Immunoprecipitation (Co-IP)

Co-IP experiments were conducted as previously described (Xie et al., 2019b). p35S-FLAG-GTL1 and a p35S-FLAG-GUS negative control were cloned into pGWB412 (Nakagawa et al., 2007) using gateway LR reactions. The following construct combinations were co-transformed into Arabidopsis mesophyll protoplasts- p35S-BES1-GFP + p35S-FLAG-GUS; p35S-FLAG-GTL1 + p35S-GFP-GUS; p35S-BES1-GFP + p35S-FLAG-GTL1. After overnight incubation, transformed protoplasts were harvested and homogenized in Co-IP buffer (50 mM Tris–HCl, pH 7.5, 150 mM NaCl, 10% (v/v) glycerol, 0.1% (v/v) Nonidet P-40, 1 mM phenylmethylsulfonyl fluoride, 20 mM MG132, and proteinase inhibitor cocktail) for 1 h at 4 °C with rotation. 5 µg FLAG M2 antibody (F1804, Sigma) was pre-bound to 40 µL protein G Dynabeads (10003D, Thermo Fisher Scientific) for 30 min in phosphate-buffered saline (PBS) buffer with 0.02% Tween 20 at room temperature. The beads were washed once with the same PBS buffer and resuspended in Co-IP buffer. After protein extraction, 10 µL of anti-FLAG pre-bound Dynabeads was added to each sample for another 1.5 h incubation at 4 °C with rotation. Dynabeads were precipitated using a DynaMagnetic rack (12321D, Thermo Fisher Scientific) and washed twice with Co-IP buffer with Nonidet P-40 and three times with Co-IP buffer without Nonidet P-40. The IP products were eluted in 2XSDS sample buffer and used for immunoblotting with

rabbit anti-GFP (A11122, Invitrogen) and rabbit anti-FLAG antibody (F7425, Sigma–Aldrich) at 1:1,000 dilution.

scRNA-seq profiling of Arabidopsis root protoplasts using the 10X Genomics chromium system

scRNA-seq experiments were performed as previously described (Shahan et al., 2022) with minor modifications. Plants were grown for 7 days as described above with the addition of 100 µm nylon mesh (Nitex 03-100/44) on the plates to facilitate root collection. For each sample, ~0.5cm root tips were harvested from 1000–3000 roots and placed into a 35mm petri dish containing a 70 µm cell strainer and 4.5mL enzyme solution (1.5% [w/v] cellulase [ONOZUKA R-10, GoldBio], 0.1% Pectolyase [Sigma P3026], 0.4 M mannitol, 20 mM MES (pH 5.7), 20 mM KCl, 10 mM CaCl₂, 0.1% bovine serum albumin, and 0.000194% (v/v) beta-mercaptoethanol). The digestion was incubated on an 85 rpm shaker at 25°C for one hour with additional stirring every 15–20 minutes. The resulting cell solution was filtered twice through 40 µm cell strainers and centrifuged for 5 minutes at 500g in a swinging bucket rotor. The pellet was washed with 2mL washing solution (0.4 M mannitol, 20 mM MES (pH 5.7), 20 mM KCl, 10 mM CaCl₂, 0.1% bovine serum albumin, and 0.000194% (v/v) beta-mercaptoethanol), centrifuged again at 500g for 3 minutes, and the pellet resuspended in washing solution at a concentration of ~2000 cells/µL. We loaded 16,000 cells, with the aim to capture 10,000 cells per sample with the 10X Genomics Chromium 3' Gene expression v3 or v3.1 kits. Cell barcoding and library construction were performed following the manufacturer's instructions. cDNA and final library quality were verified using a Bioanalyzer High Sensitivity DNA Chip (Agilent) and sequenced on an Illumina NextSeq 500 or NovaSeq 6000 instrument to produce 100bp paired-end reads.

For BL scRNA-seq, we first grew plants on 1 µM BRZ to deplete endogenous BRs, then transferred plants to either a fresh BRZ plate or 100nM BL. We monitored the efficacy of these treatments using a constitutively expressed 35S-BES1-GFP line. In agreement with previous reports (Gampala et al., 2007; Ryu et al., 2007; Yin et al., 2002), BES1-GFP was predominantly present in the cytoplasm under low BR conditions resulting from BRZ treatment but accumulated in the nucleus following BL treatment (Figure S2A). We performed two separate BL scRNA-seq treatment experiments. The first consisted of a BRZ and 2 hour BL treatment. The second experiment included two additional replicates of BRZ and BL 2 hours along with the other time points in our time course (BL 0.5, 1, 4, and 8 hour treatments). Each of the BL treatments was staggered so that all samples were collected simultaneously. A total of 70,223 cells were recovered from the BL treatment scRNA-seq experiments.

Wild type Col-0, *bril-T*, and *pGL2-BRI1-GFP/bril-T* were similarly profiled in a side-by-side scRNA-seq experiment under control conditions with two replicates per genotype, resulting in 34,861 cells. Lastly, scRNA-seq was performed on Wild type Col-0, *gtl1*, *dfl*, and *gtl1 dfl* in duplicate under control conditions, resulting in 74,810 scRNA-seq

expression profiles.

scRNA-seq data pre-processing

Raw sequencing reads were demultiplexed from Illumina BCL files to produce FASTQ files for each sample using CellRanger mkfastq (v3.1.0, 10X Genomics). Reads were then aligned against the Arabidopsis TAIR10 reference genome to generate a gene-by-cell matrix using the scKB script <https://github.com/ohlerlab/scKB>, which incorporates kallisto (Bray et al., 2016) and bustools (Melsted et al., 2019, 2021). Quality filtering of cells was performed using the R package COPILOT (Cell preprOcessing Pipeline kaLlistO busTools) (Shahan et al., 2022). COPILOT uses a non-arbitrary scheme to remove empty droplets and dying or low-quality cells. We used one iteration of COPILOT filtering, which adequately separated high-quality cells from the background in our samples based on an examination of barcode rank plots. To address issues with doublets and outliers, the resulting high-quality cells were further filtered to remove the top 1% of cells in terms of UMI counts, and putative doublets were removed with DoubletFinder using the estimated doublet rate from the 10X Genomics Chromium Single Cell 3' Reagent Kit user guide.

Normalization, annotation, and integration of scRNA-seq datasets

Downstream analysis were carried out using Seurat version 3.1.5. Samples were first individually processed and examined. Data were normalized using SCTransform (Hafemeister and Satija, 2019) and all detected genes were subsequently retained for analysis, except those from mitochondria, chloroplasts or those affected by protoplasting (absolute log2 fold-change ≥ 2) (Denyer et al., 2019; Shahan et al., 2022). Principal component analysis (PCA) was performed by calculating 50 principal components using the RunPCA function (with `approx=FALSE`). UMAP non-linear dimensionality reduction was next calculated via the RunUMAP function using all 50 principal components with parameters `n_neighbors = 30`, `min_dist = 0.3`, `umap.method = 'umap-learn'`, `metric = 'correlation'`. These processing steps have been previously described (Shahan et al., 2022) and are documented in jupyter notebooks as part of the COPILOT workflow.

To follow the developmental progression from the meristem to the elongation zone more closely, we updated the root atlas (Shahan et al., 2022) developmental annotation to subdivide the meristem into the proliferation domain and transition domain as previously defined (Ivanov and Dubrovsky, 2013). The previous meristem annotation of the root atlas was based on correlation annotation by comparing each cell from scRNA-seq to bulk data from morphologically defined sections (Brady et al., 2007). On the other hand, HIGH PLOIDY2 was used to mark the meristem in a second bulk expression profile (Li et al., 2016), which corresponds to the proliferation domain defined by Ivanov and Dubrovsky. Therefore, we leveraged correlation-based annotations derived from Li et al., 2016 to re-label the meristem of the at-

las. If cells were defined as “meristem” by both Li et al., 2016 and Brady et al., 2007, then they were re-labeled as the proliferation domain. Those that were called elongation in the Li et al., 2016 annotation, but meristem in the Brady et al., 2007 annotation were re-labeled as the transition domain. Finally, cells labeled as elongation in both Brady and Li datasets but annotated as meristem in the root atlas were re-labeled as elongation zone.

Consistent with our annotation, we found that cell cycle-related genes were enriched in the proliferation domain of the atlas (Figure S1B), whereas *SMR1* (AT3G10525), a marker of endoreduplication, increased in the transition domain (Bhosale et al., 2018). The developmental annotation of cortex markers *CO2* (AT1G62500) and *CORTEX* (AT1G09750) also matched their expression patterns in the root (Heidstra et al., 2004; Lee et al., 2006).

We used the receiver operating characteristic (ROC) test implemented in Seurat FindMarkers to identify genes enriched in each developmental zone. A largely distinct set of markers was enriched in the transition domain (Figure S1C and Data S2). These included genes involved in vesicle-mediated transport (Figure S1D), in line with the observation that vesicle recycling activity is highest in this region (Baluska et al., 2010).

We transferred the cell type and developmental stage labels from the wild-type atlas (Shahan et al., 2022) to each sample using the Seurat label transfer workflow (Butler et al., 2018; Stuart et al., 2019). To align corresponding cell types and developmental stages, we integrated samples from each experiment using the Seurat reference-based integration pipeline (Butler et al., 2018; Stuart et al., 2019). A sample from the atlas with the highest genes detected (`sc_12`) was used as a reference (Shahan et al., 2022) and two previously described samples (`dc_1` and `dc_2`) (Denyer et al., 2019) were also included in each integration. PCA and UMAP were subsequently calculated for each integration object using the batch-corrected “integrated” assay as described above. Although `sc_12`, `dc_1` and `dc_2` were not used in any subsequent analysis, their inclusion at the integration step helped to generate a comparable UMAP projection among different integration objects that facilitates interpretability.

Plotting gene expression values on the UMAP projection

We subsequently examined changes in cell state caused by the BL treatments or in the mutants profiled by plotting the log-normalized, ‘corrected’ counts produced by the SCTransform function (Hafemeister and Satija, 2019) rather than the batch-corrected “integrated” values when visualizing changes in expression.

Pseudotime estimation and heatmaps of gene expression trends

Cortex cells were extracted from the integrated Seurat objects (BR time course, *bri1-T* vs wild type and *gtl1 dfl* vs wild type). Pseudotime was then inferred on the SCT assay of the extracted cortex cells using CytoTRACE v0.1.0 (Gulati et al., 2020). Once the pseudotime was calculated,

the cortex cells were converted into SingleCellExperiment objects (Amezquita et al., 2019) before fitting a NB-GAM model (generalized additive model with a negative binomial distribution) using fitGAM function of tradeSeq R package v1.8.0 (Van den Berge et al., 2020). The model-predicted expression trends were plotted with ComplexHeatmap in R (Gu et al., 2016) (v2.10.0).

Pseudobulk differential expression analysis

Recent benchmarks point towards pseudobulk methods, which aggregate cell level counts for subpopulations of interest on a per-sample basis, as top performers for cross-condition comparisons in scRNA-seq (Crowell et al., 2020; Squair et al., 2021). Therefore, we employed a pseudobulk approach implemented in muscat (Multi-sample multi-group scRNA-seq analysis tools) (Crowell et al., 2020) to examine changes in each combination of cell type and developmental stage. Pseudobulk expression profiles were aggregated for each of these subpopulations by summing the raw counts using the aggregateData function. We then performed differential expression testing using the edgeR method (McCarthy et al., 2012) incorporated in the pbDS function. A term for the experimental batch and/or replicate was included in the contrast to adjust for potential batch effects. A gene was considered differentially expressed in a given subpopulation if the false discovery-rate adjusted p-value was ≤ 0.05 , absolute fold change was ≥ 1.5 and detection frequency was $\geq 10\%$ in one of the conditions. Gene ontology enrichment analysis was conducted on the differentially expressed genes using the R package “gprofiler2” (Kolberg et al., 2020). Comparisons between DEG lists were performed using the GeneOverlap package (version 1.12.0; <http://shenlab-sinai.github.io/shenlab-sinai/>). p-values for intersections between gene lists were computed using Fisher’s exact test. Visualizations were generated using Seurat (Stuart et al., 2019), ComplexHeatmap (Gu et al., 2016), and ggplot2 (Wickham, 2016).

WOT differential expression along cortex cell wall + trajectories

WOT constructs trajectories of cells from a reference time point by minimizing the difference over all genes (Schiebinger et al., 2019). The algorithm requires as input the expression profiles of cells as well as an estimation of their proliferation rate. We estimated proliferation rates using imaging data (Rahni and Birnbaum, 2019), as previously described (Zhang et al., 2021). As only the bottom 0.5 cm of each root was observed at each time, we expect some cells to exit the observed section due to proliferation. We estimated the number of cells that should exit the observed section based on the growth rate with the assumption that the section of root stays in equilibrium and assigned the calculated number of cells with the highest pseudotime a growth rate of zero so that they have no descendants in the observed root section at the next time point. We constructed trajectories using full gene expression profiles and evaluated the quality of the trajectories by checking the proportion of cells

whose highest fate probability matched the annotation. We found that for 90% of cells the largest fate assigned by WOT matched the annotation, rising to 97% in the maturation zone where we have the greatest confidence in the annotation. The cell wall signature was calculated for each cell by taking the sum of Z-scores for each of the 107 BR-induced cell wall-related genes in the signature (GO:0071554), truncated to $[-5,5]$. We defined the cortex cell wall+ subset as cortex cells with a cell wall score greater or equal to 1. This threshold was chosen as it selected less than 5% of cells from other lineages while still retaining $>20\%$ of cortex cells at the 2 hour time point. Any cortex cell that did not belong to the cortex cell wall+ group was labelled as “cortex cell wall-”. We performed differential expression on the cortex cell wall+ and cell wall- subsets at 2 hours, using WOT lineages to also perform differential expression on their putative ancestors and descendants. Statistical significance was evaluated using Welch’s t-Test with adjusted p-values for multiple tests, requiring $t_{FDR} < 0.01$. Results were ranked by the adjusted expression ratio

$$\frac{p_{\max}}{p_{\min} + \varepsilon}$$

with $\varepsilon = 0.1$, where larger ε puts more emphasis on genes with non-zero expression in both groups. Using the same process, we also performed differential expression between groups of cells along the same WOT trajectory at adjacent time points.

Gene regulatory networks

In order to construct GRNs, we used CellOracle (v0.7.0) for single-cell GRN inference (Kamimoto et al., 2020). In the first stage of the CellOracle pipeline, a base GRN is defined, representing a global set of biologically plausible Transcription factor-Target interactions. We used publicly available scATAC-seq data from Arabidopsis roots (Farmer et al., 2021) GSE155304:GSM4698760; (Farmer et al., 2021) to determine regions of open chromatin. Cell Ranger ATAC (v1.2.0) was used to process raw scATAC seq data to call a peak-by-cell matrix. Cicero (v1.11.1) (Pliner et al., 2018) was implemented to infer a co-accessibility map of chromatin regions. Transcription start sites were then annotated based on the Arabidopsis TAIR10 genome assembly. Finally, peaks with weak co-accessibility scores were filtered following instructions of CellOracle manual (https://morrislab.github.io/CellOracle/documentation/tutorials/base_grn.html). To expand the number of TFs present in the base GRN we also included TF-Target interactions from DNA affinity purification sequencing (DAP-seq) (Bartlett et al., 2017) and a previously constructed integrative gene regulatory network (iGRN) (De Clercq et al., 2021). Our resulting base GRN contained 11.7 million interactions between 1,601 transcription factors and 31,019 target genes.

In the second step of the CellOracle pipeline, a regularized machine learning approach is used to define active edges and their regulatory strength in clusters or subpopulations of scRNA-seq data. In this process, the expression of target genes is predicted based on regulatory transcription factor

levels from the base GRN. Inactive edges with low predictive ability are pruned from the base GRN, revealing context-specific GRN configurations (Kamimoto et al., 2020).

To test CellOracle on *Arabidopsis* root data, we first inferred GRN configurations for each of the 36 cell type and developmental stage combinations in our WT atlas (Shahan et al., 2022) using the SCT normalized counts. We limited the base GRN to genes dynamically expressed along pseudotime for each cell type plus associated transcription factors (Pruneda-Paz et al., 2014). Each cell type GRN was then constructed with default parameters following the CellOracle manual. To filter network edges with the “filter_links” function, we retained the top 20,000 edges (p-value ≤ 0.01) for each sub-network. This recovered known developmental regulators (Data S6 and Data S7) including MYB36 in the endodermis (Kamiya et al., 2015) and BRN1/BRN2 in the root cap (Bennett et al., 2010), confirming that CellOracle analysis of *Arabidopsis* root scRNA-seq data can infer GRNs configurations for particular cell identities and states.

We implemented similar procedures to infer context-specific GRN configurations for each cell type, developmental stage and time point of the BR time course samples (sc_43-50). We used transcription factors plus DEGs from BL 2 hour vs. BRZ pseudobulk analysis of each cell type/developmental zone combination. The resulting set of 201 GRN configurations spanned 767,970 edges between 1,164 transcription factors and 7,135 targets (Data S8). Network centrality measures were calculated using the built-in functions of the CellOracle pipeline (Data S9). The data needed to reproduce our results and jupyter notebooks demonstrating the processes are available on ARVEX (<https://shiny.mdc-berlin.de/ARVEX/>).

Data and code availability

Single-cell RNA-seq data have been deposited at GEO: GSE212230. All original code is available at <https://github.com/tmnolan/Brassinosteroid-gene-regulatory-networks-at-cellular-resolution>.

ACKNOWLEDGEMENTS

This work was funded by the US National Science Foundation (Postdoctoral Research Fellowships in Biology Program grant no. IOS-2010686 and MCB 1818160) to T.M.N. and Y.Y., respectively; US National Institutes of Health (NRSA postdoctoral fellowship 1F32GM136030-01 and MIRA 1R35GM131725) to R.S. and P.N.B., respectively; Research Foundation-Flanders (project no. G002121N to E.R. and a postdoctoral fellowships no. 12R7822N and no. 12R7819N to N.V.); Deutsche Forschungsgemeinschaft (International Research Training Group 2403) to C.-W.H. and U.O.; USDA-NIFA 2021-67034-35139 to I.W.T.; a Burroughs Wellcome Fund Career Award, NFRF Exploration Grant, NSERC Discovery Grant, and CIHR Project Grant to L.G., M.H., A.A., and G.S.; and by the Howard Hughes Medical Institute to P.N.B. as an Investigator. The authors thank Heather Belcher and Megan Perkins Jacobs for technical assistance; Nicolas Devos and Duke GCB for sequencing services; Nick Vangheluwe, Tom Beekman and Thomas B. Jacobs (VIB-UGent) for CRISPR-TSKO advice; and Keiko Sugimoto for *glt1* and *dfl* seeds.

AUTHOR CONTRIBUTIONS

T.M.N., N.V., C.-W.H., E.R., and P.N.B., conceptualized the experiments. T.M.N., R.S., and I.W.T. generated the scRNA-seq data. C.-W.H., T.M.N., L.G., M.H., A.A., and G.S. analyzed scRNA-seq data. N.V. and I.V. generated and characterized BRN1-TSKO lines. T.M.N. and J.Z., generated mutants using multiplex CRISPR. T.M.N., J.Z., and P.S. constructed reporter lines. T.M.N. and A.B. performed confocal imaging. P.W. performed Co-IP experiments. C.-W.H. and T.M.N. developed the ARVEX scRNA-seq browser. T.M.N. wrote the manuscript with input from all authors. Y.Y., G.S., U.O., E.R., and P.N.B. supervised the experiments and analyses.

COMPETING FINANCIAL INTERESTS

P.N.B. is the co-founder and Chair of the Scientific Advisory Board of Hi Fidelity Genetics, a company that works on crop root growth.

REFERENCES

- Ackerman-Lavert, M., and Savaldi-Goldstein, S. (2020). Growth models from a brassinosteroid perspective. *Curr. Opin. Plant Biol.* 53, 90–97. <https://doi.org/10.1016/j.pbi.2019.10.008>.
- Ackerman-Lavert, M., Fridman, Y., Matosevich, R., Khandal, H., Friedlander-Shani, L., Vragović, K., Ben El, R., Horev, G., Tarkowska, D., Efroni, I., et al. (2021). Auxin requirements for a meristematic state in roots depend on a dual brassinosteroid function. *Curr. Biol.* <https://doi.org/10.1016/j.cub.2021.07.075>.
- Aibar, S., González-Blas, C.B., Moerman, T., Huynh-Thu, V.A., Imrichova, H., Hulselmans, G., Rambow, F., Marine, J.-C., Geurts, P., Aerts, J., et al. (2017). SCENIC: single-cell regulatory network inference and clustering. *Nat. Methods* 14, 1083–1086. <https://doi.org/10.1038/nmeth.4463>.
- Amezquita, R.A., Lun, A.T.L., Becht, E., Carey, V.J., Carpp, L.N., Geistlinger, L., Martini, F., Rue-Albrecht, K., Rizzo, D., Sonesson, C., et al. (2019). Orchestrating single-cell analysis with Bioconductor. *Nat. Methods* <https://doi.org/10.1038/s41592-019-0654-x>.
- Andreou, A.I., and Nakayama, N. (2018). Mobius Assembly: A versatile Golden-Gate framework towards universal DNA assembly. *PLoS One* 13, e0189892. <https://doi.org/10.1371/journal.pone.0189892>.
- Ariel, F.D., Manavella, P.A., Dezar, C.A., and Chan, R.L. (2007). The true story of the HD-Zip family. *Trends Plant Sci.* 12, 419–426. <https://doi.org/10.1016/j.tplants.2007.08.003>.
- Asami, T., Min, Y.K., Nagata, N., Yamagishi, K., Takatsuto, S., Fujioka, S., Murofushi, N., Yamaguchi, I., and Yoshida, S. (2000). Characterization of brassinazole, a triazole-type brassinosteroid biosynthesis inhibitor. *Plant Physiol.* 123, 93–100. <https://doi.org/10.1104/pp.123.1.93>.
- Baluska, F., Mancuso, S., Volkmann, D., and Barlow, P.W. (2010). Root apex transition zone: a signalling-response nexus in the root. *Trends Plant Sci.* 15, 402–408. <https://doi.org/10.1016/j.tplants.2010.04.007>.
- Bargmann, B.O.R., Vanneste, S., Krouk, G., Nawy, T., Efroni, I., Shani, E., Choe, G., Friml, J., Bergmann, D.C., Estelle, M., et al. (2013). A map of cell type-specific auxin responses. *Mol. Syst. Biol.* 9, 688. <https://doi.org/10.1038/msb.2013.40>.
- Bartlett, A., O'Malley, R.C., Huang, S.-S.C., Galli, M., Nery, J.R., Gallavotti, A., and Ecker, J.R. (2017). Mapping genome-wide transcription-factor binding sites using DAP-seq. *Nat. Protoc.* 12, 1659–1672. <https://doi.org/10.1038/nprot.2017.055>.
- Baskin, and Jensen. (2013). On the role of stress anisotropy in the growth of stems. *J. Exp. Bot.* 4697–4707, <https://doi.org/10.1093/jxb/ert176>.
- Belkhadir, Y., and Jaillais, Y. (2015). The molecular circuitry of brassinosteroid signaling. *New Phytol.* 206, 522–540. <https://doi.org/10.1111/nph.13269>.
- Bennett, T., van den Toorn, A., Sanchez-Perez, G.F., Campilho, A., Willemsen, V., Snel, B., and Scheres, B. (2010). SOMBRETO, BEARSKIN1, and BEARSKIN2 Regulate Root Cap Maturation in *Arabidopsis*. *The Plant Cell* 22, 640–654. <https://doi.org/10.1105/tpc.109.072272>.
- Betegón-Putze, I., Mercadal, J., Bosch, N., Planas-Riverola, A., Marqués-Bueno, M., Vilarrasa-Blasi, J., Frigola, D., Burkart, R.C., Martínez, C., Conesa, A., et al. (2021). Precise transcriptional control of cellular quiescence by BRAVO/WOX5 complex in *Arabidopsis* roots. *Mol. Syst. Biol.* 17, e9864. <https://doi.org/10.15252/msb.20209864>.
- Bhosale, R., Boudolf, V., Cuevas, F., Lu, R., Eekhout, T., Hu, Z., Van Isterdael, G., Lambert, G.M., Xu, F., Nowack, M.K., et al. (2018). A Spatiotemporal DNA Endoploidy Map of the *Arabidopsis* Root Reveals Roles for the Endocycle in Root Development and Stress Adaptation. *Plant Cell* 30, 2330–2351. <https://doi.org/10.1105/tpc.17.00983>.
- Bou Daher, F., Chen, Y., Bozorg, B., Clough, J., Jönsson, H., and Braybrook, S.A. (2018). Anisotropic growth is achieved through the additive mechanical effect of material anisotropy and elastic asymmetry. *Elife* 7. <https://doi.org/10.7554/eLife.38161>.
- Brady, S.M., Orlando, D.A., Lee, J.-Y., Wang, J.Y., Koch, J., Dinneny, J.R., Mace, D., Ohler, U., and Benfey, P.N. (2007). A high-resolution root spatiotemporal map reveals dominant expression patterns. *Science* 318, 801–806. <https://doi.org/10.1126/science.1146265>.
- Bray, N.L., Pimentel, H., Melsted, P., and Pachter, L. (2016). Near-optimal probabilistic RNA-seq quantification. *Nat. Biotechnol.* 34, 525–527. <https://doi.org/10.1038/nbt.3519>.
- Breuer, C., Kawamura, A., Ichikawa, T., Tominaga-Wada, R., Wada, T., Kondou, Y., Muto, S., Matsui, M., and Sugimoto, K. (2009). The trihelix transcription factor

- GTL1 regulates ploidy-dependent cell growth in the Arabidopsis trichome. *Plant Cell* 21, 2307–2322. <https://doi.org/10.1105/tpc.109.068387>.
- Breuer, C., Morohashi, K., Kawamura, A., Takahashi, N., Ishida, T., Umeda, M., Grotewold, E., and Sugimoto, K. (2012). Transcriptional repression of the APC/C activator CCS52A1 promotes active termination of cell growth. *EMBO J.* 31, 4488–4501. <https://doi.org/10.1038/emboj.2012.294>.
- Bringmann, M., Li, E., Sampathkumar, A., Kocabek, T., Hauser, M.-T., and Persson, S. (2012). POM-POM2/cellulose synthase interacting1 is essential for the functional association of cellulose synthase and microtubules in Arabidopsis. *Plant Cell* 24, 163–177. <https://doi.org/10.1105/tpc.111.093575>.
- Butler, A., Hoffman, P., Smibert, P., Papalexi, E., and Satija, R. (2018). Integrating single-cell transcriptomic data across different conditions, technologies, and species. *Nat. Biotechnol.* 36, 411–420. <https://doi.org/10.1038/nbt.4096>.
- Caño-Delgado, A., Yin, Y., Yu, C., Vafeados, D., Mora-García, S., Cheng, J.-C., Nam, K.H., Li, J., and Chory, J. (2004). BRL1 and BRL3 are novel brassinosteroid receptors that function in vascular differentiation in Arabidopsis. *Development* 131, 5341–5351. <https://doi.org/10.1242/dev.01403>.
- Chaiwanon, J., and Wang, Z.-Y. (2015). Spatiotemporal brassinosteroid signaling and antagonism with auxin pattern stem cell dynamics in Arabidopsis roots. *Curr. Biol.* 25, 1031–1042. <https://doi.org/10.1016/j.cub.2015.02.046>.
- Cheng, Y., Zhu, W., Chen, Y., Ito, S., Asami, T., and Wang, X. (2014). Brassinosteroids control root epidermal cell fate via direct regulation of a MYB-bHLH-WD40 complex by GSK3-like kinases. *Elife* <https://doi.org/10.7554/eLife.02525>.
- Clark, N.M., Nolan, T.M., Wang, P., Song, G., Montes, C., Valentine, C.T., Guo, H., Sozzani, R., Yin, Y., and Walley, J.W. (2021). Integrated omics networks reveal the temporal signaling events of brassinosteroid response in Arabidopsis. *Nat. Commun.* 12, 5858. <https://doi.org/10.1038/s41467-021-26165-3>.
- Clough, S.J., and Bent, A.F. (1998). Floral dip: a simplified method for *Agrobacterium*-mediated transformation of *Arabidopsis thaliana*. *Plant J.* 16, 735–743. <https://doi.org/10.1046/j.1365-3113.1998.00343.x>.
- Clouse, S.D., Langford, M., and McMorris, T.C. (1996). A brassinosteroid-insensitive mutant in *Arabidopsis thaliana* exhibits multiple defects in growth and development. *Plant Physiol.* 111, 671–678. <https://doi.org/10.1104/pp.111.3.671>.
- Conant, D., Hsiao, T., Rossi, N., Oki, J., Maures, T., Waite, K., Yang, J., Joshi, S., Kelso, R., Holden, K., et al. (2022). Inference of CRISPR Edits from Sanger Trace Data. *CRISPR J* 5, 123–130. <https://doi.org/10.1089/crispr.2021.0113>.
- Crowell, H.L., Soneson, C., Germain, P.-L., Calini, D., Collin, L., Raposo, C., Malhotra, D., and Robinson, M.D. (2020). muscat detects subpopulation-specific state transitions from multi-sample multi-condition single-cell transcriptomics data. *Nat. Commun.* 11, 6077. <https://doi.org/10.1038/s41467-020-19894-4>.
- Decaestecker, W., Buono, R.A., Pfeiffer, M.L., Vangheluwe, N., Jourquin, J., Karimi, M., Van Isterdael, G., Beeckman, T., Nowack, M.K., and Jacobs, T.B. (2019). CRISPR-TSKO: A Technique for Efficient Mutagenesis in Specific Cell Types, Tissues, or Organs in Arabidopsis. *Plant Cell* 31, 2868–2887. <https://doi.org/10.1105/tpc.19.00454>.
- De Clercq, I., Van de Velde, J., Luo, X., Liu, L., Storme, V., Van Bel, M., Pottier, R., Vaneechoutte, D., Van Breusegem, F., and Vandepoele, K. (2021). Integrative inference of transcriptional networks in Arabidopsis yields novel ROS signalling regulators. *Nature Plants* 7, 500–513. <https://doi.org/10.1038/s41477-021-00894-1>.
- Denyer, T., Ma, X., Klesen, S., Scacchi, E., Nieselt, K., and Timmermans, M.C.P. (2019). Spatiotemporal Developmental Trajectories in the Arabidopsis Root Revealed Using High-Throughput Single-Cell RNA Sequencing. *Dev. Cell* 48, 840–852.e5. <https://doi.org/10.1016/j.devcel.2019.02.022>.
- Dietrich, D., Pang, L., Kobayashi, A., Fozard, J.A., Boudolf, V., Bhosale, R., Antoni, R., Nguyen, T., Hiratsuka, S., Fujii, N., et al. (2017). Root hydrotropism is controlled via a cortex-specific growth mechanism. *Nat. Plants* 3, 17057. <https://doi.org/10.1038/nplants.2017.57>.
- Dolan, L., Janmaat, K., Willemsen, V., Linstead, P., Poethig, S., Roberts, K., and Scheres, B. (1993). Cellular organisation of the Arabidopsis thaliana root. *Development* 119, 71–84. <https://doi.org/10.1242/dev.119.1.71>.
- Ebrahimi-Motlagh, S., Ribone, P.A., Thirumalaikumar, V.P., Allu, A.D., Chan, R.L., Mueller-Roeber, B., and Balazadeh, S. (2017). JUNGBRUNNEN1 Confers Drought Tolerance Downstream of the HD-Zip I Transcription Factor AtHB13. *Front. Plant Sci.* 8, 2118. <https://doi.org/10.3389/fpls.2017.02118>.
- Engler, C., Youles, M., Gruetznern, R., Ehnert, T.-M., Werner, S., Jones, J.D.G., Patron, N.J., and Marillonnet, S. (2014). A Golden Gate Modular Cloning Toolbox for Plants. *ACS Synth. Biol.* 3, 839–843. <https://doi.org/10.1021/sb4001504>.
- Fàbregas, N., Lozano-Elena, F., Blasco-Escámez, D., Tohge, T., Martínez-Andújar, C., Albacete, A., Osorio, S., Bustamante, M., Riechmann, J.L., Nomura, T., et al. (2018). Overexpression of the vascular brassinosteroid receptor BRL3 confers drought resistance without penalizing plant growth. *Nat. Commun.* 9, 4680. <https://doi.org/10.1038/s41467-018-06861-3>.
- Farmer, A., Thibivilliers, S., Ryu, K.H., Schiefelbein, J., and Libault, M. (2021). Single-nucleus RNA and ATAC sequencing reveals the impact of chromatin accessibility on gene expression in Arabidopsis roots at the single-cell level. *Mol. Plant* <https://doi.org/10.1016/j.molp.2021.01.001>.
- Feng, Z., Zhang, B., Ding, W., Liu, X., Yang, D.-L., Wei, P., Cao, F., Zhu, S., Zhang, F., Mao, Y., et al. (2013). Efficient genome editing in plants using a CRISPR/Cas system. *Cell Res.* 23, 1229–1232. <https://doi.org/10.1038/cr.2013.114>.
- Fridman, Y., Elkouby, L., Holland, N., Vragović, K., Elbaum, R., and Savaldi-Goldstein, S. (2014). Root growth is modulated by differential hormonal sensitivity in neighboring cells. *Genes Dev.* 28, 912–920. <https://doi.org/10.1101/gad.239335.114>.
- Fridman, Y., Strauss, S., Horev, G., Ackerman-Lavert, M., Reiner-Benaim, A., Lane, B., Smith, R.S., and Savaldi-Goldstein, S. (2021). The root meristem is shaped by brassinosteroid control of cell geometry. *Nature Plants* 7, 1475–1484. <https://doi.org/10.1038/s41477-021-01014-9>.
- Friedrichsen, D.M., Joazeiro, C.A., Li, J., Hunter, T., and Chory, J. (2000). Brassinosteroid-insensitive-1 is a ubiquitously expressed leucine-rich repeat receptor serine/threonine kinase. *Plant Physiol.* 123, 1247–1256. <https://doi.org/10.1104/pp.123.4.1247>.
- Gaillochet, C., Develtere, W., and Jacobs, T.B. (2020). CRISPR Screens in Plants: Approaches, Guidelines, and Future Prospects. *Plant Cell* <https://doi.org/10.1105/tpc.20.00463>.
- Gampala, S.S., Kim, T.-W., He, J.-X., Tang, W., Deng, Z., Bai, M.-Y., Guan, S., Lalonde, S., Sun, Y., Gendron, J.M., et al. (2007). An essential role for 14-3-3 proteins in brassinosteroid signal transduction in Arabidopsis. *Dev. Cell* 13, 177–189. <https://doi.org/10.1016/j.devcel.2007.06.009>.
- Gao, D., Appiano, M., Huibers, R.P., Chen, X., Loonen, A.E.H.M., Visser, R.G.F., Wolters, A.-M.A., and Bai, Y. (2014). Activation tagging of ATHB13 in Arabidopsis thaliana confers broad-spectrum disease resistance. *Plant Mol. Biol.* 86, 641–653. <https://doi.org/10.1007/s11103-014-0253-2>.
- Geng, Y., Wu, R., Wee, C.W., Xie, F., Wei, X., Chan, P.M.Y., Tham, C., Duan, L., and Dinnyen, J.R. (2013). A spatio-temporal understanding of growth regulation during the salt stress response in Arabidopsis. *Plant Cell* 25, 2132–2154. <https://doi.org/10.1105/tpc.113.112896>.
- González-García, M.-P., Vilarrasa-Blasi, J., ponova, M., Divol, F., Mora-García, S., Russinova, E., and Caño-Delgado, A.I. (2011). Brassinosteroids control meristem size by promoting cell cycle progression in Arabidopsis roots. *Development* 138, 849–859. <https://doi.org/10.1242/dev.057331>.
- Graeff, M., Rana, S., Marhava, P., Moret, B., and Hardtke, C.S. (2020). Local and Systemic Effects of Brassinosteroid Perception in Developing Phloem. *Curr. Biol.* <https://doi.org/10.1016/j.cub.2020.02.029>.
- Graeff, M., Rana, S., Wendrich, J.R., Dorier, J., Eekhout, T., Fandino, A.C.A., Guex, N., Bassel, G.W., De Rybel, B., and Hardtke, C.S. (2021). A single-cell morpho-transcriptomic map of brassinosteroid action in the Arabidopsis root. *Mol. Plant* 0. <https://doi.org/10.1016/j.molp.2021.07.021>.
- Großholz, R., Wanke, F., Glöckner, N., Rausch, L., Rohr, L., Scholl, S., Scacchi, E., Spazierer, A.-J., Shabala, L., Shabala, S., et al. (2021). Computational modeling and quantitative cell physiology reveal central parameters for the brassinosteroid-regulated cell growth of the Arabidopsis root.
- Grove, M.D., Spencer, G.F., Rohwedder, W.K., Mandava, N., Worley, J.F., Warthen, J.D., Steffens, G.L., Flippen-Anderson, J.L., and Cook, J.C. (1979). Brassinolide, a plant growth-promoting steroid isolated from *Brassica napus* pollen. *Nature* 281, 216–217. <https://doi.org/10.1038/281216a0>.
- Grützner, R., Martin, P., Horn, C., Mortensen, S., Cram, E.J., Lee-Parsons, C.W.T., Stüttmann, J., and Marillonnet, S. (2021). High-efficiency genome editing in plants mediated by a Cas9 gene containing multiple introns. *Plant Communications* 2, 100135. <https://doi.org/10.1016/j.xplc.2020.100135>.
- Gu, Y., Kaplinsky, N., Bringmann, M., Cobb, A., Carroll, A., Sampathkumar, A., Baskin, T.I., Persson, S., and Somerville, C.R. (2010). Identification of a cellulose synthase-associated protein required for cellulose biosynthesis. *Proc. Natl. Acad. Sci. U. S. A.* 107, 12866–12871. <https://doi.org/10.1073/pnas.1007092107>.

- Gu, Z., Eils, R., and Schlesner, M. (2016). Complex heatmaps reveal patterns and correlations in multidimensional genomic data. *Bioinformatics* 32, 2847–2849. <https://doi.org/10.1093/bioinformatics/btw313>.
- Guo, H., Li, L., Aluru, M., Aluru, S., and Yin, Y. (2013). Mechanisms and networks for brassinosteroid regulated gene expression. *Curr. Opin. Plant Biol.* 16, 545–553. <https://doi.org/10.1016/j.pbi.2013.08.002>.
- Gupta, A., Rico-Medina, A., and Caño-Delgado, A.I. (2020). The physiology of plant responses to drought. *Science* 368, 266–269. <https://doi.org/10.1126/science.aaz7614>.
- Hacham, Y., Holland, N., Butterfield, C., Ubeda-Tomas, S., Bennett, M.J., Chory, J., and Savaldi-Goldstein, S. (2011). Brassinosteroid perception in the epidermis controls root meristem size. *Development* 138, 839–848. <https://doi.org/10.1242/dev.061804>.
- Hafemeister, C., and Satija, R. (2019). Normalization and variance stabilization of single-cell RNA-seq data using regularized negative binomial regression. *Genome Biol.* 20, 296. <https://doi.org/10.1186/s13059-019-1874-1>.
- Harris, J.C., Hrmova, M., Lopato, S., and Langridge, P. (2011). Modulation of plant growth by HD-Zip class I and II transcription factors in response to environmental stimuli. *New Phytol.* 190, 823–837. <https://doi.org/10.1111/j.1469-8137.2011.03733.x>.
- He, Z., Wang, Z.Y., Li, J., Zhu, Q., Lamb, C., Ronald, P., and Chory, J. (2000). Perception of brassinosteroids by the extracellular domain of the receptor kinase BRI1. *Science* 288, 2360–2363. <https://doi.org/10.1126/science.288.5475.2360>.
- Heidstra, R., Welch, D., and Scheres, B. (2004). Mosaic analyses using marked activation and deletion clones dissect Arabidopsis SCARECROW action in asymmetric cell division. *Genes Dev.* 18, 1964–1969. <https://doi.org/10.1101/gad.305504>.
- Henriksson, E., Olsson, A.S.B., Johannesson, H., Johansson, H., Hanson, J., Engström, P., and Söderman, E. (2005). Homeodomain leucine zipper class I genes in Arabidopsis. Expression patterns and phylogenetic relationships. *Plant Physiol.* 139, 509–518. <https://doi.org/10.1104/pp.105.063461>.
- Holzwardt, E., Huerta, A.I., Glöckner, N., Garnelo Gómez, B., Wanke, F., Augustin, S., Askani, J.C., Schürholz, A.-K., Harter, K., and Wolf, S. (2018). BRI1 controls vascular cell fate in the Arabidopsis root through RLP44 and phytosulfokine signaling. *Proc. Natl. Acad. Sci. U. S. A.* 115, 11838–11843. <https://doi.org/10.1073/pnas.1814434115>.
- Houbaert, A., Zhang, C., Tiwari, M., Wang, K., de Marcos Serrano, A., Savatin, D.V., Urs, M.J., ponova, M.K., Gudesblat, G.E., Vanhoutte, I., et al. (2018). POLAR-guided signalling complex assembly and localization drive asymmetric cell division. *Nature* 563, 574–578. <https://doi.org/10.1038/s41586-018-0714-x>.
- Huynh-Thu, V.A., Irrthum, A., Wehenkel, L., and Geurts, P. (2010). Inferring regulatory networks from expression data using tree-based methods. *PLoS One* 5. <https://doi.org/10.1371/journal.pone.0012776>.
- Iacono, G., Massoni-Badosa, R., and Heyn, H. (2019). Single-cell transcriptomics unveils gene regulatory network plasticity. *Genome Biol.* 20, 110. <https://doi.org/10.1186/s13059-019-1713-4>.
- Irani, N.G., Di Rubbo, S., Mylle, E., Van den Begin, J., Schneider-Pizor, J., Hnilková, J., Šiša, M., Buyst, D., Vilarasa-Blasi, J., Szatmári, A.-M., et al. (2012). Fluorescent castasterone reveals BRI1 signaling from the plasma membrane. *Nat. Chem. Biol.* 8, 583–589. <https://doi.org/10.1038/nchembio.958>.
- Ivanov, V.B., and Dubrovsky, J.G. (2013). Longitudinal zonation pattern in plant roots: conflicts and solutions. *Trends Plant Sci.* 18, 237–243. <https://doi.org/10.1016/j.tplants.2012.10.002>.
- Iyer-Pascuzzi, A.S., Jackson, T., Cui, H., Petricka, J.J., Busch, W., Tsukagoshi, H., and Benfey, P.N. (2011). Cell identity regulators link development and stress responses in the Arabidopsis root. *Dev. Cell* 21, 770–782. <https://doi.org/10.1016/j.devcel.2011.09.009>.
- Jaillais, Y., and Vert, G. (2016). Brassinosteroid signaling and BRI1 dynamics went underground. *Curr. Opin. Plant Biol.* 33, 92–100. <https://doi.org/10.1016/j.pbi.2016.06.014>.
- Jaillais, Y., Belkhadir, Y., Balsemão-Pires, E., Dangl, J.L., and Chory, J. (2011). Extracellular leucine-rich repeats as a platform for receptor/coreceptor complex formation. *Proc. Natl. Acad. Sci. U. S. A.* 108, 8503–8507. <https://doi.org/10.1073/pnas.1103556108>.
- Jean-Baptiste, K., McFaline-Figueroa, J.L., Alexandre, C.M., Dorrity, M.W., Saunders, L., Bubb, K.L., Trapnell, C., Fields, S., Queitsch, C., and Cuperus, J.T. (2019). Dynamics of Gene Expression in Single Root Cells of Arabidopsis thaliana. *Plant Cell* 31, 993–1011. <https://doi.org/10.1105/tpc.18.00785>.
- Kamimoto, K., Hoffmann, C.M., and Morris, S.A. (2020). CellOracle: Dissecting cell identity via network inference and in silico gene perturbation.
- Kamiya, T., Borghi, M., Wang, P., Danku, J.M.C., Kalmbach, L., Hosmani, P.S., Naseer, S., Fujiwara, T., Geldner, N., and Salt, D.E. (2015). The MYB36 transcription factor orchestrates Casparian strip formation. *Proc. Natl. Acad. Sci. U. S. A.* 112, 10533–10538. <https://doi.org/10.1073/pnas.1507691112>.
- Kang, Y.H., Breda, A., and Hardtke, C.S. (2017). Brassinosteroid signaling directs formative cell divisions and protophloem differentiation in Arabidopsis root meristems. *Development* 144, 272–280. <https://doi.org/10.1242/dev.145623>.
- Kinoshita, T., Caño-Delgado, A., Seto, H., Hiranuma, S., Fujioka, S., Yoshida, S., and Chory, J. (2005). Binding of brassinosteroids to the extracellular domain of plant receptor kinase BRI1. *Nature* 433, 167–171. <https://doi.org/10.1038/nature03227>.
- Kolberg, L., Raudvere, U., Kuzmin, I., Vilo, J., and Peterson, H. (2020). gprofiler2 -- an R package for gene list functional enrichment analysis and namespace conversion toolset g:Profiler. *F1000Research* 9, 709. <https://doi.org/10.12688/f1000research.24956.1>.
- Kuppusamy, K.T., Chen, A.Y., and Nemhauser, J.L. (2009). Steroids are required for epidermal cell fate establishment in Arabidopsis roots. *Proc. Natl. Acad. Sci. U. S. A.* 106, 8073–8076. <https://doi.org/10.1073/pnas.0811633106>.
- Labun, K., Montague, T.G., Krause, M., Torres Cleuren, Y.N., Tjeldnes, H., and Valen, E. (2019). CHOPCHOP v3: expanding the CRISPR web toolbox beyond genome editing. *Nucleic Acids Res.* 47, W171–W174. <https://doi.org/10.1093/nar/gkz365>.
- Lee, J.-Y., Colinas, J., Wang, J.Y., Mace, D., Ohler, U., and Benfey, P.N. (2006). Transcriptional and posttranscriptional regulation of transcription factor expression in Arabidopsis roots. *Proc. Natl. Acad. Sci. U. S. A.* 103, 6055–6060. <https://doi.org/10.1073/pnas.0510607103>.
- Levine, M., and Davidson, E.H. (2005). Gene regulatory networks for development. *Proc. Natl. Acad. Sci. U. S. A.* 102, 4936–4942. <https://doi.org/10.1073/pnas.0408031102>.
- Li, J., and Chory, J. (1997). A putative leucine-rich repeat receptor kinase involved in brassinosteroid signal transduction. *Cell* 90, 929–938. [https://doi.org/10.1016/s0092-8674\(00\)80357-8](https://doi.org/10.1016/s0092-8674(00)80357-8).
- Li, J., Nagpal, P., Vitart, V., McMorris, T.C., and Chory, J. (1996). A role for brassinosteroids in light-dependent development of Arabidopsis. *Science* 272, 398–401. <https://doi.org/10.1126/science.272.5260.398>.
- Li, J., Wen, J., Lease, K.A., Doke, J.T., Tax, F.E., and Walker, J.C. (2002). BAK1, an Arabidopsis LRR receptor-like protein kinase, interacts with BRI1 and modulates brassinosteroid signaling. *Cell* 110, 213–222. [https://doi.org/10.1016/s0092-8674\(02\)00812-7](https://doi.org/10.1016/s0092-8674(02)00812-7).
- Li, L., Yu, X., Thompson, A., Guo, M., Yoshida, S., Asami, T., Chory, J., and Yin, Y. (2009). Arabidopsis MYB30 is a direct target of BES1 and cooperates with BES1 to regulate brassinosteroid-induced gene expression. *Plant J.* 58, 275–286. <https://doi.org/10.1111/j.1365-313X.2008.03778.x>.
- Li, S., Lei, L., Somerville, C.R., and Gu, Y. (2012). Cellulose synthase interactive protein 1 (CSI1) links microtubules and cellulose synthase complexes. *Proc. Natl. Acad. Sci. U. S. A.* 109, 185–190. <https://doi.org/10.1073/pnas.1118560109>.
- Li, S., Yamada, M., Han, X., Ohler, U., and Benfey, P.N. (2016). High-Resolution Expression Map of the Arabidopsis Root Reveals Alternative Splicing and lincRNA Regulation. *Dev. Cell* 39, 508–522. <https://doi.org/10.1016/j.devcel.2016.10.012>.
- Li, Z., Sela, A., Fridman, Y., Garstka, L., Höfte, H., Savaldi-Goldstein, S., and Wolf, S. (2021). Optimal BR signalling is required for adequate cell wall orientation in the Arabidopsis root meristem. *Development* 148. <https://doi.org/10.1242/dev.199504>.
- Longkumer, T., Chen, C.-Y., Biancucci, M., Bhaskara, G.B., and Verslues, P.E. (2021). Spatial differences in stoichiometry of EGR phosphatase and Microtubule-Associated Stress Protein 1 control root meristem activity during drought stress. *Plant Cell* <https://doi.org/10.1093/plcell/koab290>.
- Lozano-Elena, F., Planas-Riverola, A., Vilarasa-Blasi, J., Schwab, R., and Caño-Delgado, A.I. (2018). Paracrine brassinosteroid signaling at the stem cell niche controls cellular regeneration. *J. Cell Sci.* 131. <https://doi.org/10.1242/jcs.204065>.
- Mabuchi, K., Maki, H., Itaya, T., Suzuki, T., Nomoto, M., Sakaoka, S., Morikami, A., Higashiyama, T., Tada, Y., Busch, W., et al. (2018). MYB30 links ROS signaling, root cell elongation, and plant immune responses. *Proc. Natl. Acad. Sci. U. S. A.* 115, E4710–E4719. <https://doi.org/10.1073/pnas.1804233115>.
- Marbach, D., Costello, J.C., Küffner, R., Vega, N.M., Prill, R.J., Camacho, D.M., Allison, K.R., DREAM5 Consortium, Kellis, M., Collins, J.J., et al. (2012). Wisdom of crowds for robust gene network inference. *Nat. Methods* 9, 796–804.

<https://doi.org/10.1038/nmeth.2016>.

Marquès-Bueno, M.D.M., Morao, A.K., Cayrel, A., Platre, M.P., Barberon, M., Caillieux, E., Colot, V., Jaillais, Y., Roudier, F., and Vert, G. (2016). A versatile Multisite Gateway-compatible promoter and transgenic line collection for cell type-specific functional genomics in Arabidopsis. *Plant J.* **85**, 320–333. <https://doi.org/10.1111/tpj.13099>.

Mattsson, J., Söderman, E., Svenson, M., Borkird, C., and Engström, P. (1992). A new homeobox-leucine zipper gene from Arabidopsis thaliana. *Plant Mol. Biol.* **18**, 1019–1022. <https://doi.org/10.1007/BF00019223>.

McCarthy, D.J., Chen, Y., and Smyth, G.K. (2012). Differential expression analysis of multifactor RNA-Seq experiments with respect to biological variation. *Nucleic Acids Res.* **40**, 4288–4297. <https://doi.org/10.1093/nar/gks042>.

Melsted, P., Ntranos, V., and Pachter, L. (2019). The barcode, UMI, set format and BUStools. *Bioinformatics* **35**, 4472–4473. <https://doi.org/10.1093/bioinformatics/btz279>.

Melsted, P., Boeshaghi, A.S., Liu, L., Gao, F., Lu, L., Min, K.H.J., da Veiga Beltrame, E., Hjörleifsson, K.E., Gehring, J., and Pachter, L. (2021). Modular, efficient and constant-memory single-cell RNA-seq preprocessing. *Nat. Biotechnol.* **39**, 813–818. <https://doi.org/10.1126/sciadv.abd4113>.

Miao, R., Yuan, W., Wang, Y., Garcia-Maquilon, I., Dang, X., Li, Y., Zhang, J., Zhu, Y., Rodriguez, P.L., and Xu, W. (2021). Low ABA concentration promotes root growth and hydrotropism through relief of ABA INSENSITIVE 1-mediated inhibition of plasma membrane H⁺-ATPase 2. *Science Advances* **7**, eabd4113. <https://doi.org/10.1126/sciadv.abd4113>.

Moreno-Risueno, M.A., Busch, W., and Benfey, P.N. (2010). Omics meet networks—using systems approaches to infer regulatory networks in plants. *Curr. Opin. Plant Biol.* **13**, 126–131. <https://doi.org/10.1016/j.pbi.2009.11.005>.

Moreno-Risueno, M.A., Sozzani, R., Yardimci, G.G., Petricka, J.J., Vernoux, T., Bilou, I., Alonso, J., Winter, C.M., Ohler, U., Scheres, B., et al. (2015). Transcriptional control of tissue formation throughout root development. *Science* **350**, 426–430. <https://doi.org/10.1126/science.1261171>.

Nakagawa, T., Suzuki, T., Murata, S., Nakamura, S., Hino, T., Maeo, K., Tabata, R., Kawai, T., Tanaka, K., Niwa, Y., et al. (2007). Improved Gateway binary vectors: high-performance vectors for creation of fusion constructs in transgenic analysis of plants. *Biosci. Biotechnol. Biochem.* **71**, 2095–2100. <https://doi.org/10.1271/bbb.70216>.

Nolan, T.M., Brennan, B., Yang, M., Chen, J., Zhang, M., Li, Z., Wang, X., Bassham, D.C., Walley, J., and Yin, Y. (2017). Selective Autophagy of BES1 Mediated by DSK2 Balances Plant Growth and Survival. *Dev. Cell* **41**, 33–46.e7. <https://doi.org/10.1016/j.devcel.2017.03.013>.

Nolan, T.M., Vukašinović, N., Liu, D., Russinova, E., and Yin, Y. (2020). Brassinosteroids: Multidimensional Regulators of Plant Growth, Development, and Stress Responses. *Plant Cell* **32**, 295–318. <https://doi.org/10.1105/tpc.19.00335>.

Oh, E., Zhu, J.-Y., Bai, M.-Y., Arenhart, R.A., Sun, Y., and Wang, Z.-Y. (2014). Cell elongation is regulated through a central circuit of interacting transcription factors in the Arabidopsis hypocotyl. *Elife* **3**. <https://doi.org/10.7554/eLife.03031>.

Pavelescu, I., Vilarrasa-Blasi, J., Planas-Riverola, A., González-García, M.-P., Caño-Delgado, A.I., and Ibañez, M. (2018). A Sizer model for cell differentiation in Arabidopsis thaliana root growth. *Mol. Syst. Biol.* **14**, e7687. <https://doi.org/10.15252/msb.20177687>.

Perotti, M.F., Ribone, P.A., Cabello, J.V., Ariel, F.D., and Chan, R.L. (2019). AtHB23 participates in the gene regulatory network controlling root branching, and reveals differences between secondary and tertiary roots. *Plant J.* **100**, 1224–1236. <https://doi.org/10.1111/tpj.14511>.

Perotti, M.F., Arce, A.L., Ariel, F.D., Figueroa, C.M., and Chan, R.L. (2021). The transcription factor AtHB23 modulates starch turnover for root development and plant survival under salinity.

Pierre-Jerome, E., Drapek, C., and Benfey, P.N. (2018). Regulation of Division and Differentiation of Plant Stem Cells. *Annu. Rev. Cell Dev. Biol.* **34**, 289–310. <https://doi.org/10.1146/annurev-cellbio-100617-062459>.

Planas-Riverola, A., Gupta, A., Betegón-Putze, I., Bosch, N., Ibañez, M., and Caño-Delgado, A.I. (2019). Brassinosteroid signaling in plant development and adaptation to stress. *Development* **146**. <https://doi.org/10.1242/dev.151894>.

Pliner, H.A., Packer, J.S., McFaline-Figueroa, J.L., Cusanovich, D.A., Daza, R.M., Aghamirzaie, D., Srivatsan, S., Qiu, X., Jackson, D., Minkina, A., et al. (2018). Cicero Predicts cis-Regulatory DNA Interactions from Single-Cell Chromatin Accessibility Data. *Mol. Cell* **71**, 858–871.e8. <https://doi.org/10.1016/j.molcel.2018.06.044>.

Pratapa, A., Jaliha, A.P., Law, J.N., Bharadwaj, A., and Murali, T.M. (2020). Benchmarking algorithms for gene regulatory network inference from single-cell transcriptomic data. *Nat. Methods* **17**, 147–154. <https://doi.org/10.1038/s41592-019-0690-6>.

Pruned-Paz, J.L., Breton, G., Nagel, D.H., Kang, S.E., Bonaldi, K., Doherty, C.J., Ravelo, S., Galli, M., Ecker, J.R., and Kay, S.A. (2014). A genome-scale resource for the functional characterization of Arabidopsis transcription factors. *Cell Rep.* **8**, 622–632. <https://doi.org/10.1016/j.celrep.2014.06.033>.

Rahni, R., and Birnbaum, K.D. (2019). Week-long imaging of cell divisions in the Arabidopsis root meristem. *Plant Methods* **15**, 30. <https://doi.org/10.1186/s13007-019-0417-9>.

Ribone, P.A., Capella, M., and Chan, R.L. (2015). Functional characterization of the homeodomain leucine zipper I transcription factor AtHB13 reveals a crucial role in Arabidopsis development. *J. Exp. Bot.* **66**, 5929–5943. <https://doi.org/10.1093/jxb/erv302>.

Ryu, H., Kim, K., Cho, H., Park, J., Choe, S., and Hwang, I. (2007). Nucleocytoplasmic shuttling of BZR1 mediated by phosphorylation is essential in Arabidopsis brassinosteroid signaling. *Plant Cell* **19**, 2749–2762. <https://doi.org/10.1105/tpc.107.053728>.

Ryu, K.H., Huang, L., Kang, H.M., and Schiefelbein, J. (2019). Single-Cell RNA Sequencing Resolves Molecular Relationships Among Individual Plant Cells. *Plant Physiol.* **179**, 1444–1456. <https://doi.org/10.1104/pp.18.01482>.

Sakaoka, S., Mabuchi, K., Morikami, A., and Tsukagoshi, H. (2018). MYB30 regulates root cell elongation under abscisic acid signaling. *Commun. Integr. Biol.* **11**, e1526604. <https://doi.org/10.1080/19420889.2018.1526604>.

Salvi, E., Di Mambro, R., and Sabatini, S. (2020). Dissecting mechanisms in root growth from the transition zone perspective. *J. Exp. Bot.* **71**, 2390–2396. <https://doi.org/10.1093/jxb/eraa079>.

Schiebinger, G. (2021). Reconstructing developmental landscapes and trajectories from single-cell data. *Current Opinion in Systems Biology* **27**, 100351. <https://doi.org/10.1016/j.coisb.2021.06.002>.

Schiebinger, G., Shu, J., Tabaka, M., Cleary, B., Subramanian, V., Solomon, A., Gould, J., Liu, S., Lin, S., Berube, P., et al. (2019). Optimal-Transport Analysis of Single-Cell Gene Expression Identifies Developmental Trajectories in Reprogramming. *Cell* **176**, 1517. <https://doi.org/10.1016/j.cell.2019.02.026>.

Schindelin, J., Arganda-Carreras, I., Frise, E., Kaynig, V., Longair, M., Pietzsch, T., Preibisch, S., Rueden, C., Saalfeld, S., Schmid, B., et al. (2012). Fiji: an open-source platform for biological-image analysis. *Nat. Methods* **9**, 676–682. <https://doi.org/10.1038/nmeth.2019>.

Serrano-Ron, L., Cabrera, J., Perez-Garcia, P., and Moreno-Risueno, M.A. (2021). Unraveling Root Development Through Single-Cell Omics and Reconstruction of Gene Regulatory Networks. *Front. Plant Sci.* **12**, 661361. <https://doi.org/10.3389/fpls.2021.661361>.

Seyed Rahmani, R., Shi, T., Zhang, D., Gou, X., Yi, J., Miclotte, G., Marchal, K., and Li, J. (2021). Genome-wide expression and network analyses of mutants in key brassinosteroid signaling genes. *BMC Genomics* **22**, 465. <https://doi.org/10.1186/s12864-021-07778-w>.

Seyferth, C., Renema, J., Wendrich, J.R., Eekhout, T., Seurinck, R., Vandamme, N., Blob, B., Saey, Y., Helariutta, Y., Birnbaum, K.D., et al. (2021). Advances and Opportunities of Single-Cell Transcriptomics for Plant Research. *Annu. Rev. Plant Biol.* <https://doi.org/10.1146/annurev-arplant-081720-010120>.

Shahan, R., Nolan, T.M., and Benfey, P.N. (2021). Single-cell analysis of cell identity in the Arabidopsis root apical meristem: insights and opportunities. *J. Exp. Bot.* <https://doi.org/10.1093/jxb/erab228>.

Shahan, R., Hsu, C.-W., Nolan, T.M., Cole, B.J., Taylor, I.W., Greenstreet, L., Zhang, S., Afanassiev, A., Vlot, A.H.C., Schiebinger, G., et al. (2022). A single-cell Arabidopsis root atlas reveals developmental trajectories in wild-type and cell identity mutants. *Dev. Cell* <https://doi.org/10.1016/j.devcel.2022.01.008>.

Shani, E., Weinstain, R., Zhang, Y., Castillejo, C., Kaiserli, E., Chory, J., Tsien, R.Y., and Estelle, M. (2013). Gibberellins accumulate in the elongating endodermal cells of Arabidopsis root. *Proc. Natl. Acad. Sci. U. S. A.* **110**, 4834–4839. <https://doi.org/10.1073/pnas.1300436110>.

Shibata, M., Breuer, C., Kawamura, A., Clark, N.M., Rymen, B., Braidwood, L., Morohashi, K., Busch, W., Benfey, P.N., Sozzani, R., et al. (2018). GTL1 and DF1 regulate root hair growth through transcriptional repression of ROOT HAIR DEFECTIVE 6-LIKE 4 in Arabidopsis. *Development* **145**. <https://doi.org/10.1242/dev.159707>.

- Shibata, M., Favero, D.S., Takebayashi, R., Kawamura, A., Rymen, B., Hosokawa, Y., and Sugimoto, K. (2021). GTL1 is required for a robust root hair growth response to avoid nutrient overloading.
- Shimada, T.L., Shimada, T., and Hara-Nishimura, I. (2010). A rapid and non-destructive screenable marker, FAST, for identifying transformed seeds of *Arabidopsis thaliana*. *Plant J.* 61, 519–528. <https://doi.org/10.1111/j.1365-3113.2009.04060.x>.
- Shulze, C.N., Cole, B.J., Ciobanu, D., Lin, J., Yoshinaga, Y., Gouran, M., Turco, G.M., Zhu, Y., O'Malley, R.C., Brady, S.M., et al. (2019). High-Throughput Single-Cell Transcriptome Profiling of Plant Cell Types. *Cell Rep.* 27, 2241–2247.e4. <https://doi.org/10.1016/j.celrep.2019.04.054>.
- Silva, A.T., Ribone, P.A., Chan, R.L., Ligterink, W., and Hilhorst, H.W.M. (2016). A Predictive Coexpression Network Identifies Novel Genes Controlling the Seed-to-Seedling Phase Transition in *Arabidopsis thaliana*. *Plant Physiol.* 170, 2218–2231. <https://doi.org/10.1104/pp.15.01704>.
- Squair, J.W., Gautier, M., Kathe, C., Anderson, M.A., James, N.D., Hutson, T.H., Hudelle, R., Qaiser, T., Matson, K.J.E., Barraud, Q., et al. (2021). Confronting false discoveries in single-cell differential expression. *Nat. Commun.* 12, 5692. <https://doi.org/10.1038/s41467-021-25960-2>.
- Stuart, T., Butler, A., Hoffman, P., Hafemeister, C., Papalexi, E., Mauck, W.M., 3rd, Hao, Y., Stoeckius, M., Smibert, P., and Satija, R. (2019). Comprehensive Integration of Single-Cell Data. *Cell* 177, 1888–1902.e21. <https://doi.org/10.1016/j.cell.2019.05.031>.
- Stuttman, J., Barthel, K., Martin, P., Ordon, J., Erickson, J.L., Herr, R., Ferik, F., Kretschmer, C., Berner, T., Keilwagen, J., et al. (2021). Highly efficient multiplex editing: one-shot generation of 8x *Nicotiana benthamiana* and 12x *Arabidopsis* mutants. *Plant J.* 106, 8–22. <https://doi.org/10.1111/tpj.15197>.
- Sun, Y., Fan, X.-Y., Cao, D.-M., Tang, W., He, K., Zhu, J.-Y., He, J.-X., Bai, M.-Y., Zhu, S., Oh, E., et al. (2010). Integration of brassinosteroid signal transduction with the transcription network for plant growth regulation in *Arabidopsis*. *Dev. Cell* 19, 765–777. <https://doi.org/10.1016/j.devcel.2010.10.010>.
- Swift, J., Greenham, K., Ecker, J.R., Coruzzi, G.M., and McClung, C.R. (2021). The biology of time: dynamic responses of cell types to developmental, circadian, and environmental cues. *Plant J.* <https://doi.org/10.1111/tpj.15589>.
- Szekeres, M., Németh, K., Koncz-Kálmán, Z., Mathur, J., Kauschmann, A., Altmann, T., Rédei, G.P., Nagy, F., Schell, J., and Koncz, C. (1996). Brassinosteroids rescue the deficiency of CYP90, a cytochrome P450, controlling cell elongation and de-etiolation in *Arabidopsis*. *Cell* 85, 171–182. [https://doi.org/10.1016/s0092-8674\(00\)81094-6](https://doi.org/10.1016/s0092-8674(00)81094-6).
- Takahashi, N., Goto, N., Okada, K., and Takahashi, H. (2002). Hydrotropism in abscisic acid, wavy, and gravitropic mutants of *Arabidopsis thaliana*. *Planta* 216, 203–211. <https://doi.org/10.1007/s00425-002-0840-3>.
- Ubeda-Tomás, S., Swarup, R., Coates, J., Swarup, K., Laplace, L., Beemster, G.T.S., Hedden, P., Bhaleerao, R., and Bennett, M.J. (2008). Root growth in *Arabidopsis* requires gibberellin/DELLA signalling in the endodermis. *Nat. Cell Biol.* 10, 625–628. <https://doi.org/10.1038/ncb1726>.
- Ubeda-Tomás, S., Federici, F., Casimiro, I., Beemster, G.T.S., Bhaleerao, R., Swarup, R., Doerner, P., Haseloff, J., and Bennett, M.J. (2009). Gibberellin signaling in the endodermis controls *Arabidopsis* root meristem size. *Curr. Biol.* 19, 1194–1199. <https://doi.org/10.1016/j.cub.2009.06.023>.
- Van den Berge, K., Roux de Bézieux, H., Street, K., Saelens, W., Cannoodt, R., Saeys, Y., Dudoit, S., and Clement, L. (2020). Trajectory-based differential expression analysis for single-cell sequencing data. *Nat. Commun.* 11, 1201. <https://doi.org/10.1038/s41467-020-14766-3>.
- Vanholme, R., Cesarino, I., Rataj, K., Xiao, Y., Sundin, L., Goeminne, G., Kim, H., Cross, J., Morreel, K., Araujo, P., et al. (2013). Caffeoyl shikimate esterase (CSE) is an enzyme in the lignin biosynthetic pathway in *Arabidopsis*. *Science* 341, 1103–1106. <https://doi.org/10.1126/science.1241602>.
- Verlues, P.E., and Longkumer, T. (2022). Size and activity of the root meristem: a key for drought resistance and a key model of drought-related signaling. *Physiol. Plant.* 174, e13622. <https://doi.org/10.1111/ppl.13622>.
- Vilarrasa-Blasi, J., González-García, M.-P., Frigola, D., Fàbregas, N., Alexiou, K.G., López-Bigas, N., Rivas, S., Jauneau, A., Lohmann, J.U., Benfey, P.N., et al. (2014). Regulation of plant stem cell quiescence by a brassinosteroid signaling module. *Dev. Cell* 30, 36–47. <https://doi.org/10.1016/j.devcel.2014.05.020>.
- Vragović, K., Sela, A., Friedlander-Shani, L., Fridman, Y., Hacham, Y., Holland, N., Bartom, E., Mockler, T.C., and Savaldi-Goldstein, S. (2015). Translatome analyses capture of opposing tissue-specific brassinosteroid signals orchestrating root meristem differentiation. *Proceedings of the National Academy of Sciences* 112, 923–928. .
- Vukašinović, N., Wang, Y., Vanhoutte, I., Fendrych, M., Guo, B., Kvasnica, M., Jiroutová, P., Oklestkova, J., Strnad, M., and Russinova, E. (2021). Local brassinosteroid biosynthesis enables optimal root growth. *Nat Plants* 7, 619–632. <https://doi.org/10.1038/s41477-021-00917-x>.
- Wang, X., Ye, L., Lyu, M., Ursache, R., Löytynoja, A., and Mähönen, A.P. (2020). An inducible genome editing system for plants. *Nat Plants* 6, 766–772. <https://doi.org/10.1038/s41477-020-0695-2>.
- Wang, Z.Y., Nakano, T., Gendron, J., He, J., Chen, M., Vafeados, D., Yang, Y., Fujioka, S., Yoshida, S., Asami, T., et al. (2002). Nuclear-localized BZR1 mediates brassinosteroid-induced growth and feedback suppression of brassinosteroid biosynthesis. *Dev. Cell* 2, 505–513. [https://doi.org/10.1016/s1534-5807\(02\)00153-3](https://doi.org/10.1016/s1534-5807(02)00153-3).
- von Wangenheim, D., Hauschild, R., Fendrych, M., Barone, V., Benková, E., and Friml, J. (2017). Live tracking of moving samples in confocal microscopy for vertically grown roots. *Elife* 6. <https://doi.org/10.7554/eLife.26792>.
- Wei, Z., and Li, J. (2016). Brassinosteroids Regulate Root Growth, Development, and Symbiosis. *Mol. Plant* 9, 86–100. <https://doi.org/10.1016/j.molp.2015.12.003>.
- Wendrich, J.R., Yang, B., Vandamme, N., Verstaen, K., Smet, W., Van de Velde, C., Minne, M., Wybouw, B., Mor, E., Arents, H.E., et al. (2020). Vascular transcription factors guide plant epidermal responses to limiting phosphate conditions. *Science* 370. <https://doi.org/10.1126/science.aay4970>.
- Wickham, H. (2016). ggplot2: Elegant Graphics for Data Analysis.
- Xie, L., Yang, C., and Wang, X. (2011). Brassinosteroids can regulate cellulose biosynthesis by controlling the expression of CESA genes in *Arabidopsis*. *J. Exp. Bot.* 62, 4495–4506. <https://doi.org/10.1093/jxb/err164>.
- Xie, Z., Nolan, T.M., Jiang, H., and Yin, Y. (2019a). AP2/ERF Transcription Factor Regulatory Networks in Hormone and Abiotic Stress Responses in *Arabidopsis*. *Front. Plant Sci.* 10, 228. <https://doi.org/10.3389/fpls.2019.00228>.
- Xie, Z., Nolan, T., Jiang, H., Tang, B., Zhang, M., Li, Z., and Yin, Y. (2019b). The AP2/ERF Transcription Factor TINY Modulates Brassinosteroid-Regulated Plant Growth and Drought Responses in *Arabidopsis*. *Plant Cell* 31, 1788–1806. <https://doi.org/10.1105/tpc.18.00918>.
- Ye, H., Liu, S., Tang, B., Chen, J., Xie, Z., Nolan, T.M., Jiang, H., Guo, H., Lin, H.-Y., Li, L., et al. (2017). RD26 mediates crosstalk between drought and brassinosteroid signalling pathways. *Nat. Commun.* 8, 14573. <https://doi.org/10.1038/ncomms14573>.
- Yin, Y., Wang, Z.-Y., Mora-Garcia, S., Li, J., Yoshida, S., Asami, T., and Chory, J. (2002). BES1 Accumulates in the Nucleus in Response to Brassinosteroids to Regulate Gene Expression and Promote Stem Elongation. *Cell* 109, 181–191. [https://doi.org/10.1016/S0092-8674\(02\)00721-3](https://doi.org/10.1016/S0092-8674(02)00721-3).
- Yin, Y., Vafeados, D., Tao, Y., Yoshida, S., Asami, T., and Chory, J. (2005). A new class of transcription factors mediates brassinosteroid-regulated gene expression in *Arabidopsis*. *Cell* 120, 249–259. <https://doi.org/10.1016/j.cell.2004.11.044>.
- Yu, X., Li, L., Zola, J., Aluru, M., Ye, H., and Foudree, A. (2011). A brassinosteroid transcriptional network revealed by genome-wide identification of BES1 target genes in *Arabidopsis thaliana*. *The Plant Journal*.
- Zhang, S., Afanassiev, A., Greenstreet, L., Matsumoto, T., and Schiebinger, G. (2021). Optimal transport analysis reveals trajectories in steady-state systems. *PLoS Comput. Biol.* 17, e1009466. <https://doi.org/10.1371/journal.pcbi.1009466>.
- Zhang, T.-Q., Xu, Z.-G., Shang, G.-D., and Wang, J.-W. (2019). A Single-Cell RNA Sequencing Profiles the Developmental Landscape of *Arabidopsis* Root. *Mol. Plant* 12, 648–660. <https://doi.org/10.1016/j.molp.2019.04.004>.
- Zhiponova, M.K., Morohashi, K., Vanhoutte, I., Machemer-Noonan, K., Revalska, M., Van Montagu, M., Grotewold, E., and Russinova, E. (2014). Helix-loop-helix/basic helix-loop-helix transcription factor network represses cell elongation in *Arabidopsis* through an apparent incoherent feed-forward loop. *Proc. Natl. Acad. Sci. U. S. A.* 111, 2824–2829. <https://doi.org/10.1073/pnas.1400203111>.

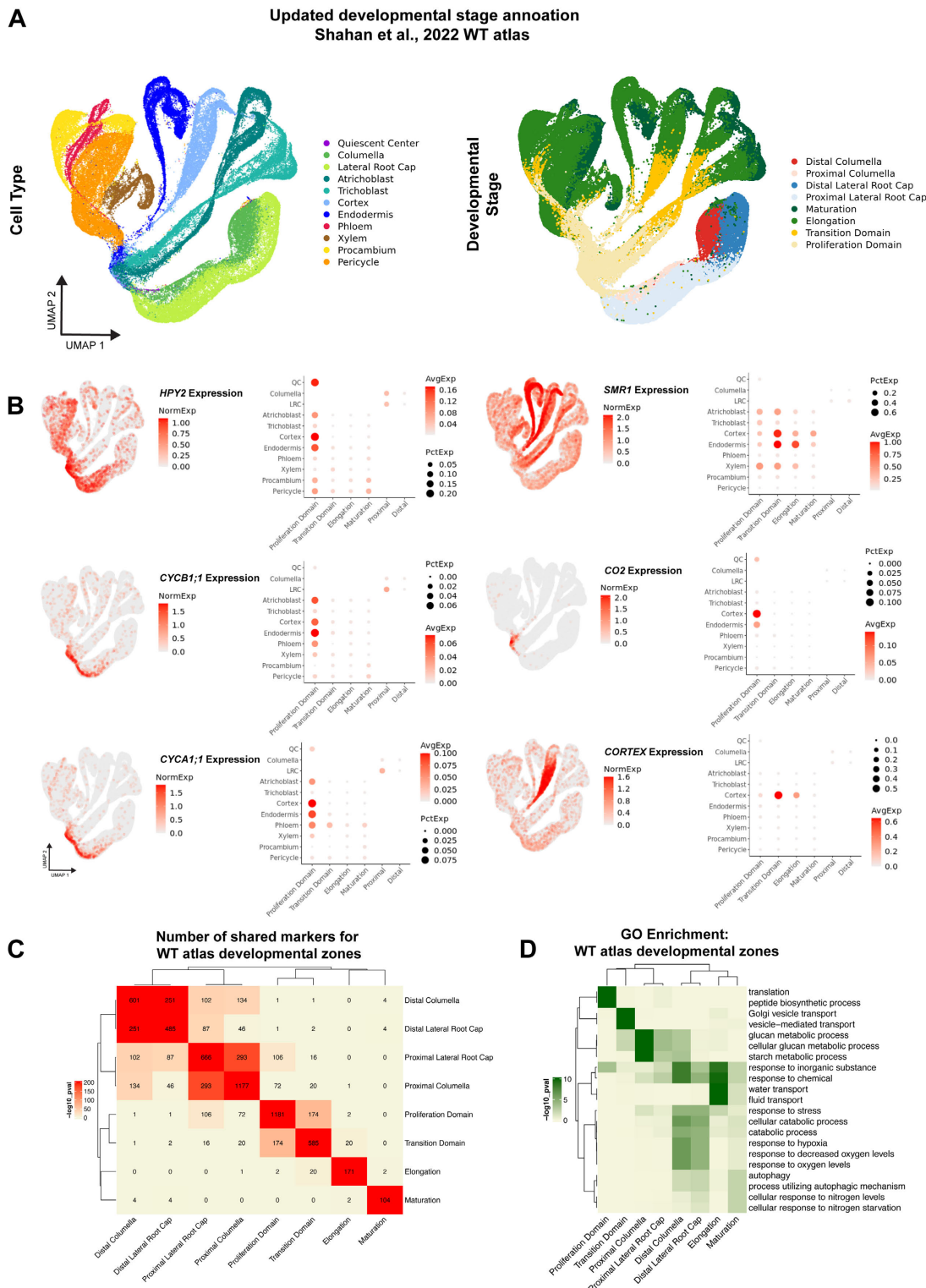


Fig. S1. Updated developmental annotation distinguishes between the proliferation domain and transition domain of the meristem. Related to Figure 1.

(A) Wild-type atlas of the Arabidopsis root from (Shahan et al., 2022) showing updated developmental stage annotation in which the meristem is divided into the proliferation domain and transition domain.

(B) Expression of markers in wild-type atlas supporting the developmental stage annotation. The color scale on the UMAP projection represents log normalized, corrected UMI counts. In dotplots, the size of the dot represents the percentage of cells in which the gene is expressed.

(C) Comparison of the number of shared markers for each of the developmental zones in the wild-type atlas. Color represents log₁₀ p-values from the indicated overlaps calculated from Fisher's exact test by GeneOverlap. The number of genes in each intersection is indicated inside each box.

(D) Enriched GO terms for markers of each developmental zone in the wild-type atlas.

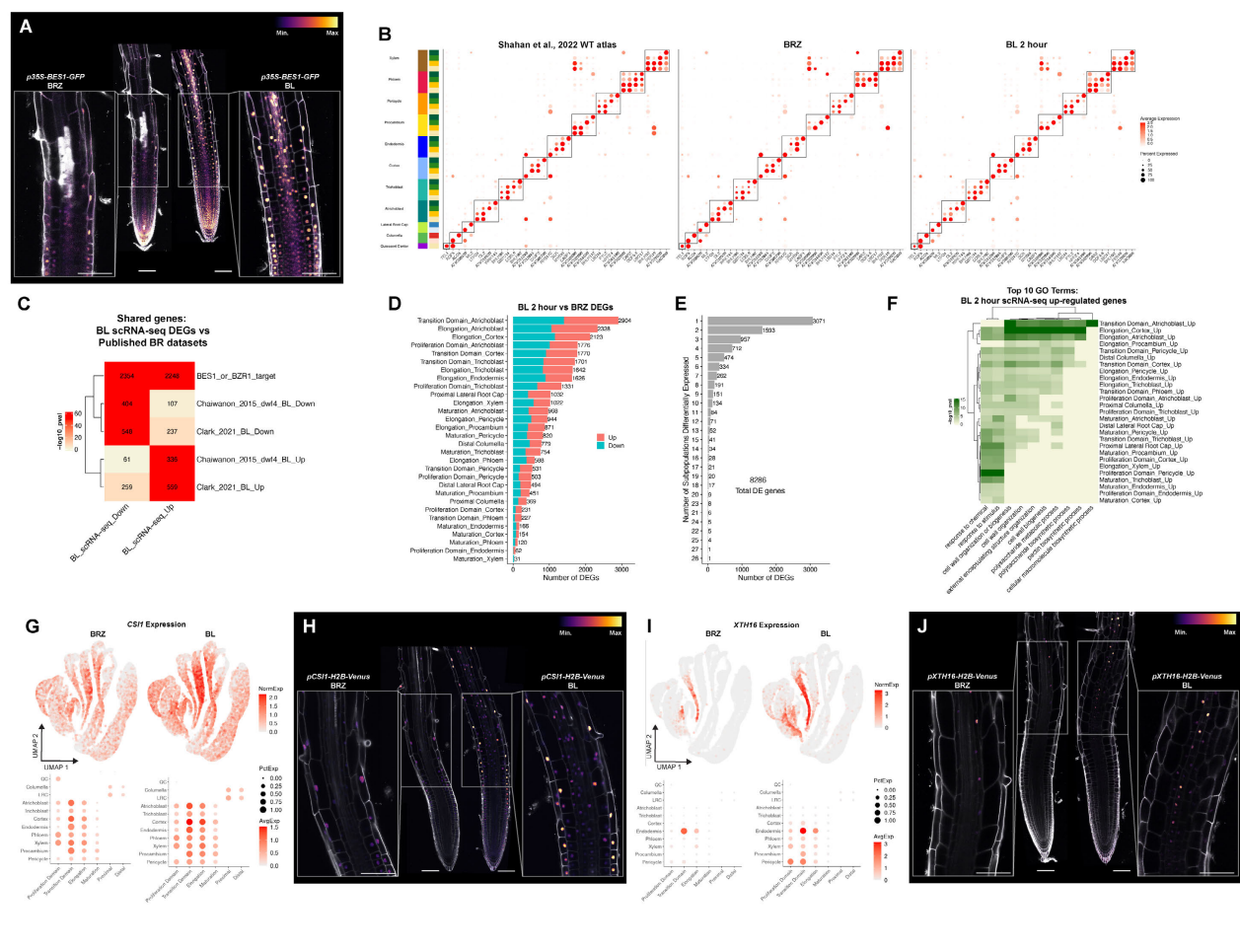


Fig. S2. scRNA-seq identifies the elongating cortex as a site of BR-response. Related to Figure 1.

(A) p35S-BES1-GFP was used to monitor the efficacy of the sensitized system for BL scRNA-seq. Plants were grown for 7 days on 1 μ M BRZ to deplete endogenous BRs, then transferred plants to either a fresh BRZ plate or 100nM BL. BES1-GFP was predominantly present in the cytoplasm under low BR conditions resulting from BRZ treatment but accumulated in the nucleus following BL treatment.

(B) Dotplots from the WT root atlas, BRZ, and BL 2 hours scRNA-seq showing that cell types and developmental stages are identified through label transfer. One marker gene for each cell type and developmental stage combination is shown. Circle size represents the percentage of cells in which a gene is expressed and color represents the average expression level of each gene. Black boxes denote markers from each cell type. Colors of side annotations indicate cell type and developmental stage.

(C) Comparison of BL 2 hour DEGs from scRNA-seq to BES1 and BZR1 ChIP targets and previous bulk BR RNA-seq datasets. Color represents log10 p-values from the indicated overlaps calculated from Fisher's exact test by GeneOverlap. The number of genes in each intersection is indicated inside each box.

(D) Number of DEGs for each cell type/developmental stage combination in BL 2 hour scRNA-seq. Color indicates the number of up-regulated vs down-regulated genes.

(E) The number of cell type/developmental stage combinations (subpopulations) in which each BL DEG is differentially expressed. 3,071/8,286 DEGs were significantly altered in only a single sub-population.

(F) Top 10 GO terms among BL up-regulated DEGs from scRNA-seq. Note the strong enrichment for cell wall-related GO terms in BL up-regulated genes in the elongating cortex.

(G) CS11 expression in BL scRNA-seq data. The color scale on the UMAP projection represents log normalized, corrected UMI counts. In dotplots, the size of the dot represents the percentage of cells in which the gene is expressed.

(H) CS11-H2B-Venus reporter grown on 1 μ M BRZ for 7 days and transferred to 1 μ M BRZ or 100nM BL for 4 hours. Inset shows CS11 signals that are strongest in cortex and epidermis and increase with BL treatment. Propidium iodide-staining is shown in grey, with the color gradient indicating relative CS11-H2B-Venus levels. Scale bars, 100 μ m.

(I) XTH16 expression in BL scRNA-seq data. The color scale on the UMAP projection represents log normalized, corrected UMI counts. In dotplots, the size of the dot represents the percentage of cells in which the gene is expressed.

(J) XTH16-H2B-Venus reporter grown on 1 μ M BRZ for 7 days and transferred to 1 μ M BRZ or 100nM BL for 4 hours. Inset shows XTH16 signals in the endodermis that increase with BL treatment. Propidium iodide-staining is shown in grey, with the color gradient indicating relative XTH16-H2B-Venus levels. Scale bars, 100 μ m.

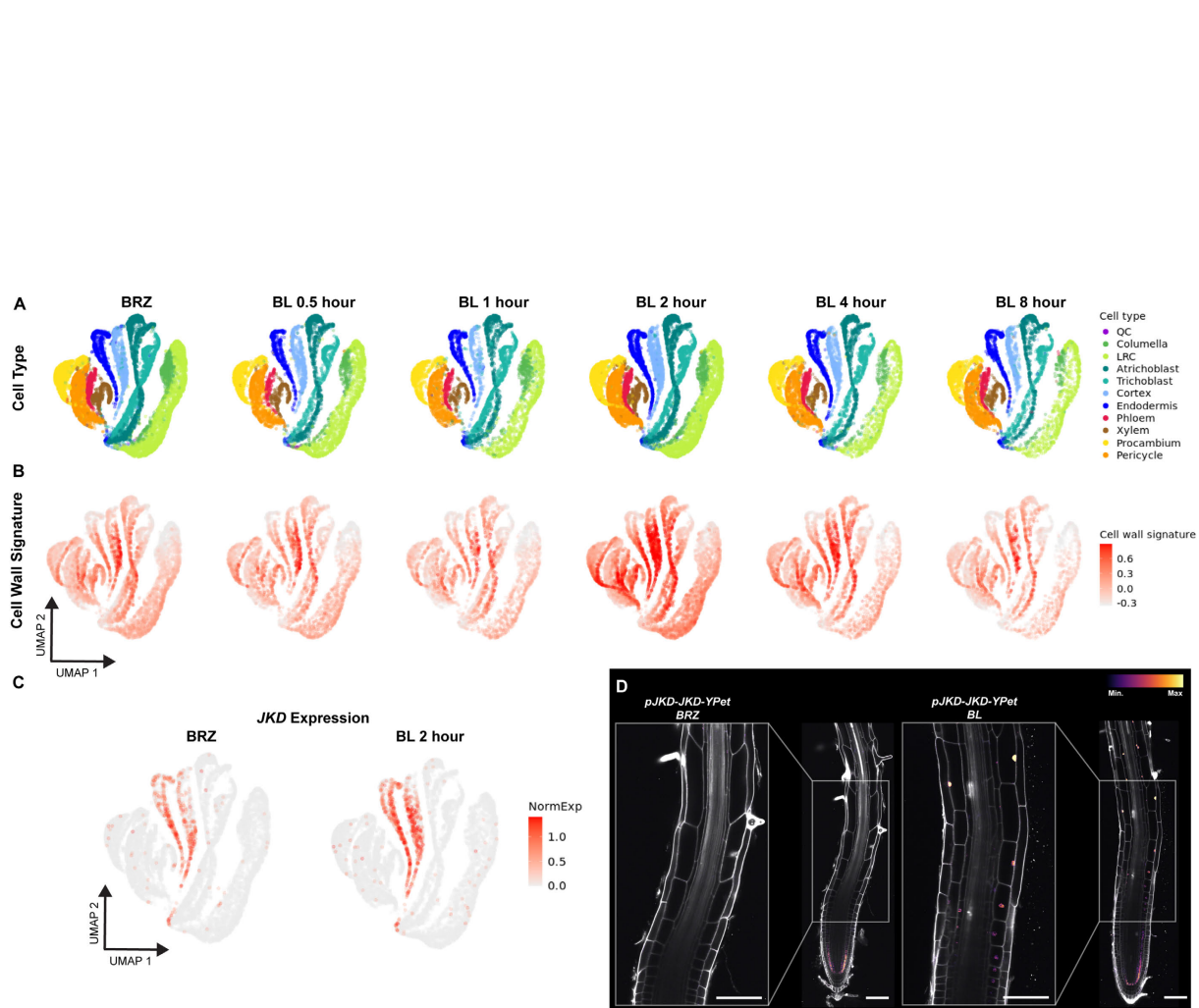


Fig. S3. Waddington optimal transport identifies JKD as a BR responsive transcription factor along cortex trajectories. Related to Figure 2.

(A) UMAP showing cell type annotation across BL scRNA-seq treatment time course. This panel is repeated from the main text figure as a reference for the panel below.
 (B) UMAP projection colored by cell wall signature, calculated as the sum of Z-scores for each of the 107 BR-induced cell wall-related genes in the signature (GO:0071554), truncated to [-5,5].
 (C) Expression of JKD in BRZ and BL 2 hour scRNA-seq. The color scale represents log normalized, corrected UMI counts.
 (D) pJKD-JKD-YPet grown on 1 μ M BRZ for 7 days and transferred to 1 μ M BRZ or 100nM BL for 4 hours. Inset shows JKD signals in the elongating cortex that increase with BL treatment. Propidium iodide-staining is shown in grey, with the color gradient indicating relative JKD-Ypet levels. Scale bars, 100 μ m.

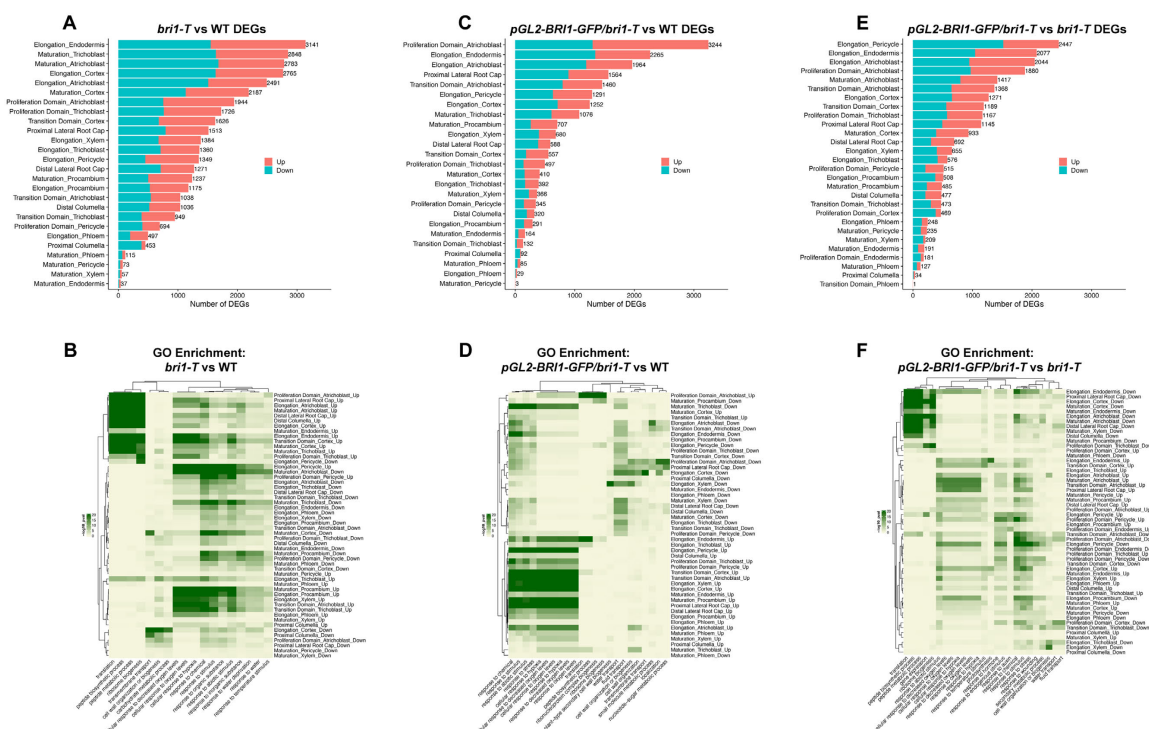


Fig. S4. Analysis of the triple receptor mutant *bri1-T* reveals changes in cortex expression and distinct gene expression patterns of *pGL2-BRI1-GFP/bri1-T*. Related to Figure 3.

(A) Number of DEGs for each cell type/developmental stage combination in *bri1-T* scRNA-seq compared to WT. Color indicates the number of up-regulated vs down-regulated genes.

(B) GO enrichment of *bri1-T* vs wild-type DEGs.

(C) Number of DEGs for each cell type/developmental stage combination in *pGL2-BRI1-GFP/bri1-T* scRNA-seq compared to WT. Color indicates the number of up-regulated vs down-regulated genes.

(D) GO enrichment of *pGL2-BRI1-GFP/bri1-T* vs wild-type DEGs.

(E) Number of DEGs for each cell type/developmental stage combination in *pGL2-BRI1-GFP/bri1-T* scRNA-seq compared to *bri1-T*. Color indicates the number of up-regulated vs down-regulated genes.

(F) GO enrichment of *pGL2-BRI1-GFP/bri1-T* vs *bri1-T* DEGs.

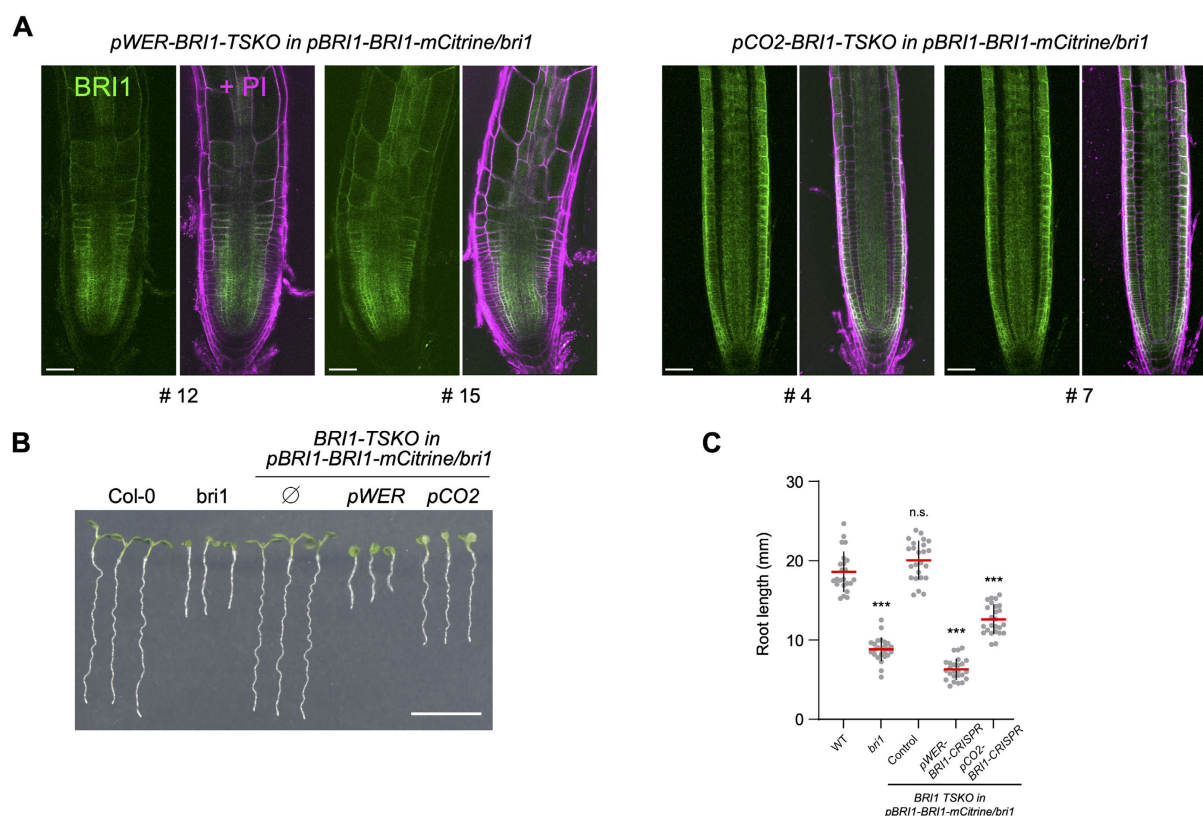


Fig. S5. BRI1 CRISPR TSKO. Related to Figure 4.

(A) Two individual transgenic lines for pWER-BRI1-CRISPR and pCO2-BRI1-CRISPR exhibiting similar BRI1-mCitrine expression patterns. Scale bars, 50 μm.

(B) Seven-day-old BRI1-TSKO transgenic seedlings with roots shorter than those of the wild-type (Col-0) control and complemented pBRI1-BRI1-mCitrine/bri1. Scale bar represents 1 cm.

(C) Quantification of the root length of transgenic lines shown in (B). All individual data points are plotted. Red horizontal bars represent the means and error bars represent s.d. Significant differences between transgenic lines and the WT control were determined by one-way ANOVA and Dunnett's multiple comparisons tests. ***P<0.001, **P<0.01, *P<0.05. n.s. not significant.

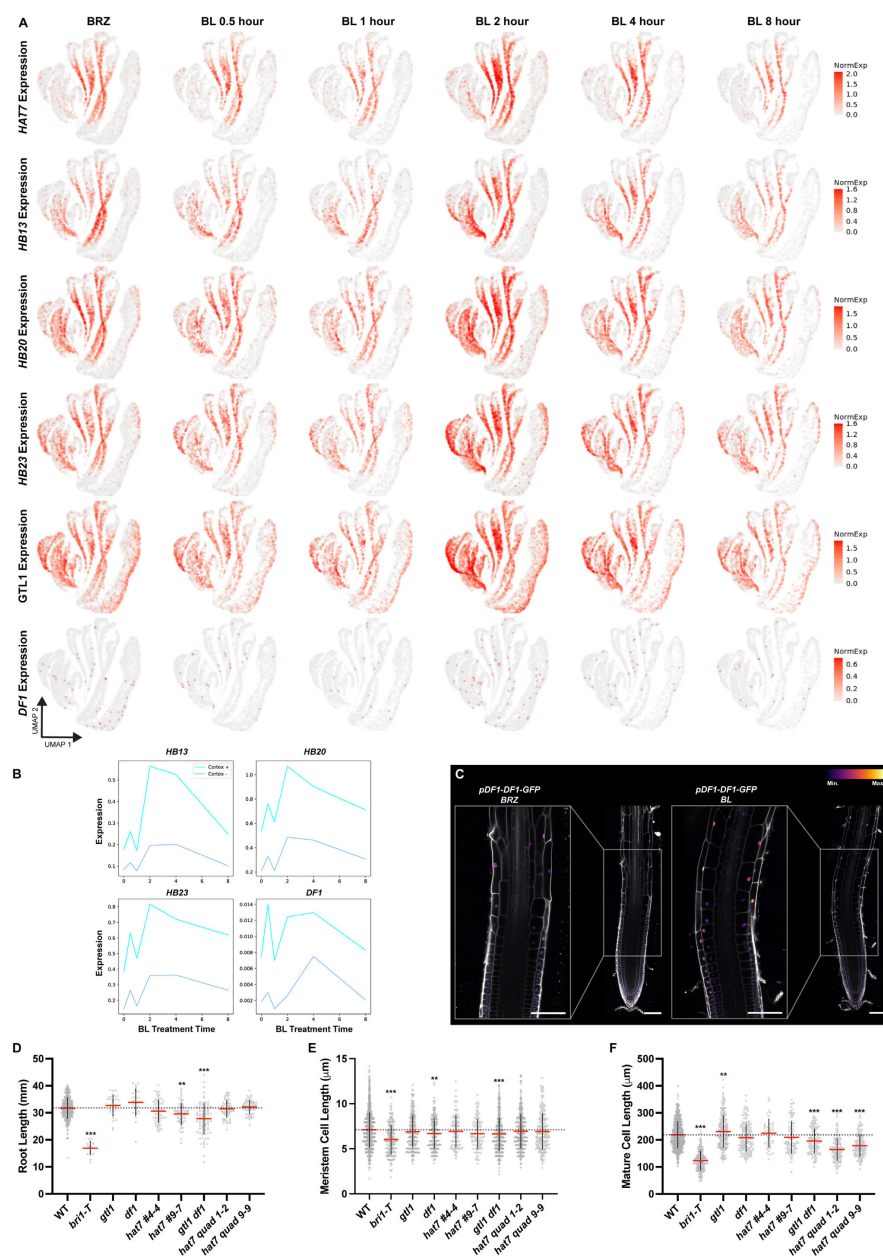


Fig. S6. HAT7 and GTL1 family transcription factors are BR responsive regulators along cortex trajectories. Related to Figure 5 and Figure 6.

(A) UMAP projections showing expression levels of HAT7 and GTL1 family transcription factors over the BR time series scRNA-seq experiment. The color scale represents log normalized, corrected UMI counts.

(B) Expression trends for indicated transcription factors along WOT cortex cell wall + (cortex +) vs cortex cell wall - (cortex -) trajectories.

(C) pDF1-DF1-GFP grown on 1 μ M BRZ for 7 days and transferred to 1 μ M BRZ or 100nM BL for 4 hours. Inset shows DF1 signals in the elongating epidermis and cortex that increase with BL treatment. Propidium iodide-staining is shown in grey, with the color gradient indicating relative DF1-GFP levels. Scale bars, 100 μ m.

(D) Quantification of the root length in the indicated mutants. hat7 quad 1-2 and 9-9 represent two independent CRISPR mutants of hat7 hb13 hb20 hb23. hat7 quad 1-2 is used as a representative allele throughout the manuscript unless otherwise indicated.

(E) Quantification of meristematic cortex cell length, defined as the first 20 cells of individual roots starting from the quiescent center.

(F) Quantification of mature cortex cell length. For D-F, all individual data points are plotted. Red horizontal bars represent the means and error bars represent s.d. Significant differences between mutants and the wild-type control were determined by one-way ANOVA and Dunnett's multiple comparisons tests. ***P<0.001, **P<0.01, *P<0.05.

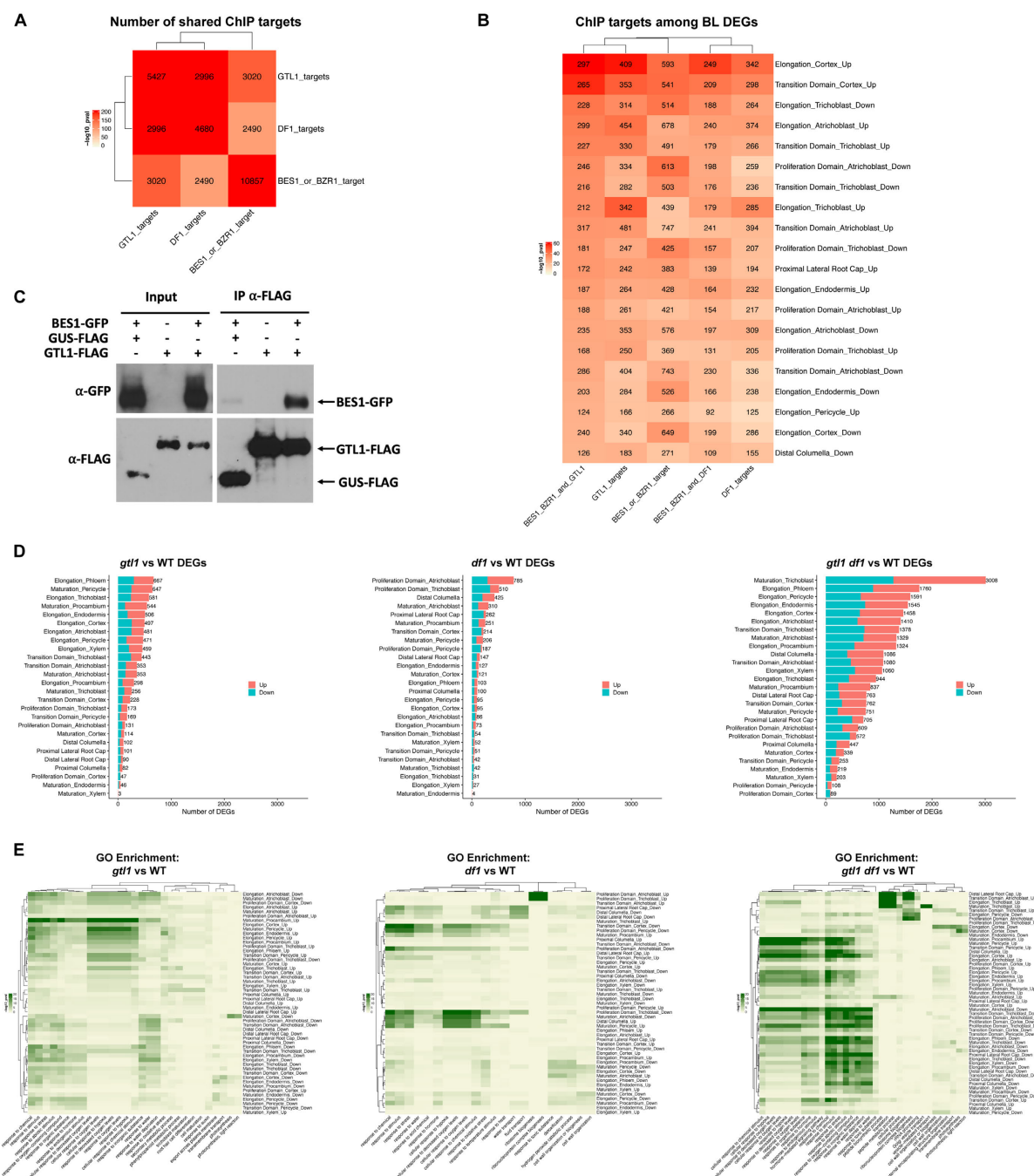


Fig. S7. BES1 and GTL1 interact and share a common set of target genes. Related to Figure 7.

(A) Comparison of BES1 or BZR1, GTL1, and DF1 ChIP targets showing an overrepresentation of shared target genes.

(B) Comparison of ChIP targets from (A) with BL 2 hour vs BRZ DEGs. The top 20 cell type/developmental stage combinations that are enriched for BES1 or BZR1 and GTL1 shared targets are shown. For (A) and (B) color represents log₁₀ p-values from the indicated overlaps calculated from Fisher's exact test by GeneOverlap. The number of genes in each intersection is indicated inside each box.

(C) Co-Immunoprecipitation demonstrating BES1 interaction with GTL1. GTL1-FLAG immunoprecipitated with anti-FLAG beads pulled down BES1-GFP, whereas a GUS-FLAG negative control did not.

(D) Number of DEGs for each cell type/developmental stage combination in *gtl1*, *df1* or *gtl1 df1* scRNA-seq compared to WT. Color indicates the number of up-regulated vs down-regulated genes.

(E) GO enrichment of DEGs in *gtl1*, *df1* or *gtl1 df1* scRNA-seq compared to WT.

Supplemental Tables

Data S1. Summary of the scRNA-seq samples reported in this study. Related to Figure 1.

Data S2. Marker genes for updated developmental annotation of Shahan et al WT root atlas. Related to Figure 1.

Data S3. DEGs from pseudobulk analysis of scRNA-seq datasets. Related to Figure 1, Figure 3, and Figure 7.

Data S4. DEGs from WOT analysis of cortex cell wall + scRNA-seq datasets. Related to Figure 2.

Data S5. DEGs from WOT analysis of each cell type and developmental stage from BR time series scRNA-seq. Related to Figure 2.

Data S6. CellOracle GRN inferred from wild-type atlas. Related to Figure 6.

Data S7. CellOracle GRN centrality metrics from wild-type atlas. Related to Figure 6.

Data S8. CellOracle GRN inferred from BR time series. Related to Figure 6.

Data S9. CellOracle GRN centrality metrics from BR time series. Related to Figure 6.

Data S10. Predicted targets of HAT7 and GTL1 family TFs from elongating cortex CellOracle GRNs in BR time series. Related to Figure 6.

Data S11. Oligos used in this study.

Video S1. Time-lapse confocal microscopy showing *pC/VIF2-H2B-Venus* in wild-type and *gtl1 df1*.

Note that Supplemental data that exceeds the file size limit can be found at:

<https://shiny.mdc-berlin.de/ARVEX/>